Ultrafast Science
A SCIENCE PARTNER JOURNAL

REVIEW ARTICLE

Recent Advances and Perspective of Photonic Bound States in the Continuum

Guizhen Xu†, Hongyang Xing†, Zhanqiang Xue†, Dan Lu, Jinying Fan, Junxing Fan*, Perry Ping Shum, and Longqing Cong*

Department of Electrical and Electronic Engineering, Southern University of Science and Technology, Shenzhen 518055, China.

*Address correspondence to: conglq@sustech.edu.cn (L.C.); fanjx@sustech.edu.cn (Junxing F.)
†These authors contributed equally to this work.

Citation: Xu G, Xing H, Xue Z, Lu D, Fan J, Shum PP, Junxing Fan, Cong L. Recent Advances and Perspective of Photonic Bound States in the Continuum. *Ultrafast Sci.* 2023;3:Article 0033. https://doi.org/10.34133/ultrafastscience.0033

Submitted 7 April 2023
Accepted 2 June 2023
Published 23 June 2023

Recent advancements in photonic bound states in the continuum (BICs) have opened up exciting new possibilities for the design of optoelectronic devices with improved performance. In this perspective article, we provide an overview of recent progress in photonic BICs based on metamaterials and photonic crystals, focusing on both the underlying physics and their practical applications. The first part of this article introduces 2 different interpretations of BICs, based on far-field interference of multipoles and near-field analysis of topological charges. We then discuss recent research on manipulating the far-field radiation properties of BICs through engineering topological charges. The second part of the article summarizes recent developments in the applications of BICs, including chiral light and vortex beam generation, nonlinear optical frequency conversion, sensors, and nanolasers. Finally, we conclude with a discussion of the potential of photonic BICs to advance terahertz applications in areas such as generation and detection, modulation, sensing, and isolation. We believe that continued research in this area will lead to exciting new advancements in optoelectronics, particularly in the field of terahertz devices.

Introduction

Bound states in the continuum (BICs) are a ubiquitous wave phenomenon in various areas such as electromagnetism, acoustics, and fluid mechanics [1]. As trapped states with embedded eigenvalues, BICs exhibit intriguing localized energy in an open resonator or non-Hermitian system, even though the system is coupled to radiation continuum [2]. The first study of BIC dates back to 1929 when von Neumann and Wigner mathematically proposed an artificial quantum potential to support a BIC [3]. In 1985, BIC was found in a 2-resonator system by continuous parameter tuning where destructive interference of the 2 resonances leads to vanishing linewidth in one of the resonances [4]. This type of BICs is known as Friedrich–Wintgen BICs or accidental BICs. The physics of BICs was not introduced to optics until 2008 [5] and then experimentally demonstrated with an array of coupled optical waveguides in 2011 where an antisymmetric mode was shown to propagate without loss to the continuum [6]. This type of BICs was known as symmetry-protected BICs that are decoupled to the continuum due to symmetry mismatch. Two years later, optical BICs were experimentally observed in a 2-dimensional (2D) periodic photonic lattice—photonic crystal (PhC), by researchers from Massachusetts Institute of Technology, which initiates the deeper exploration of BICs in PhCs and metamaterials [2].

Theoretically, BICs possess infinite radiative lifetimes in an infinitely periodic lattice enabling boundless enhancement of electric and magnetic fields. However, the finite extent of periodic lattices, intrinsic material absorption, fabrication defects, and structural disorders would result in a collapse of the divergent quality factor (Q). A leaky mode termed as "quasi-BIC" is commonly adopted for photonic applications [7]. Since ideal BICs only exist in theory and cannot be captured in far field in practice, BICs and quasi-BICs usually refer to similar leaky scenarios in the literature. It is important to note that the measured Q from a Fano resonance enabled by BIC refers to the total quality factors (Q^{tot}) contributed by radiative Q^{rad} and nonradiative Q^{nrad}, and it is thus crucial to reduce nonradiative losses for a larger Q^{tot}.

BICs are a fascinating phenomenon in PhCs and metasurfaces. Over the past few decades, BICs have been established in various photonic structures, and the fundamental physical mechanisms have been explored from different perspectives. Rapid development was witnessed in this field including fundamental physics and applications in various disciplines. There are thus numerous high-quality review articles summarizing the progress of BICs [8–10], among which a comprehensive review of BICs was reported in [11]. However, most previous research progress as well as review articles focused on photonic BICs, and the perspective of BICs on terahertz (THz) photonics is missing. We believe that the very interesting physics of BICs will have a substantial impact on developing THz technologies. In this perspective article, we will provide an outlook of BICs on THz photonics after introducing the most recent research progress in terms of interesting physics and applications. We focus on 2 types of BICs: symmetry-protected and accidental BICs. They can be observed in a band above a light cone at

high-symmetry points and nonzero wave vectors (Fig. 1A) [6,12,13]. Fundamentally, the origin of BICs is explained by destructive interference. Specifically, diffraction orders form the discretized radiation channels to a finite number of directions in a periodic lattice, and only a single open diffraction channel remains when the lattice is constructed with subwavelength unit cells [7]. BICs are formed when the coupling of the single channel to free space is ceased due to symmetry mismatch (symmetry-protected BICs) or by continuous parameter tuning (accidental BICs).

The physical interpretation of BICs in periodic lattices can be categorized into 2 directions: multipolar analysis and topological defects [14,15]. Multipolar analysis refers to the associated radiation patterns of multipoles as illustrated in the top panel of Fig. 1B, where any leakage of energy is forbidden in the normal direction if all the multipoles are not allowed to radiate along the z-axis, leading to a symmetry-protected BIC at the Γ point in the momentum space [14]. In contrast, accidental BICs can be formed when all the contributed multipoles are real and interfere destructively in the direction of $\boldsymbol{k}_1$, resulting in complete cancellation of radiation along the $\boldsymbol{k}_1$ direction of the open diffraction channel.

From the perspective of topological defects, BICs were accurately manipulated in the platform of PhCs [15,16]. As a typical open photonic system, PhCs have demonstrated a variety of applications in laser cavities [17–22], waveguides [23], and sensors [24–26] whose physical frameworks are beyond Hermitian systems. One unique feature in the non-Hermitian systems is BIC, which has no counterparts in the Hermitian systems [27]. From the polarization vector fields in momentum space, BICs are considered as topological defects whose polarization vectors are undefined. Topological defects could be numerically characterized by a topological charge (q) representing the nontrivial winding patterns of certain parameters, e.g., velocity, phase, or polarization in real space [15,28]. Specifically, for BICs in non-Hermitian systems, the topological charge is characterized by the winding of polarization vectors in momentum space as

$$q = \frac{1}{2}\oint_C dk \cdot \nabla_k \theta(k).$$

Here, $\theta(k)$ indicates the angle of major axes of the polarization vectors in momentum space that forms mode of the radiation field $\psi(k) = arg\left[e_x\hat{x} + ie_y\hat{y}\right]$, and C indicates a closed integration path to circle the state in the counterclockwise direction. According to the polarization vectors of radiation fields, a BIC renders a polarization singularity in the momentum space attributed to cancellation of radiation [15]. Since the polarization vector is not continuously defined, a nontrivial topological invariant $q \in \mathbb{Z}$ appears in analogy to a Chern number characterizing the nontrivial bulk band in a topological insulator. As a conserved and quantized quantity, topological charges are merely allowed to continuously evolve in the momentum space and remain constant unless the charge moves out of light cone or annihilates with an opposite sign charge. Such an interpretation of BICs has been experimentally demonstrated by directly observing the polarization vortices in the vicinity of mode center [29–31] and found promising applications in engineering the robustness of BICs, vortex lasers, and chiral BICs (refer to Applications).

Engineering BICs from Topological Charges

Merging BICs

Topological charges carry important characteristics of radiation, and the manipulation of them enables a flexible approach to tailor the radiation properties. Robustness is an important hallmark in the topological systems, in which the invariability is commonly prescribed for commensurate topological invariants of photonic bands mapping to momentum space such as Zak phase, Chern number, and winding number [32–35]. In this section, we will discuss recent advance in enhancing the robustness of BICs by manipulating their topological charges.

By virtue of the topological properties, a square lattice PhC slab was proposed to investigate the topological polarization singularity in momentum space [28]. In this work, a band with a BIC located at the Γ point that is guaranteed by the C_2 symmetry, as well as 8 accidental BICs located at off-Γ points, was studied. The polarization vectors were calculated to carry a topological charge of +1 or −1 at the 9 BICs, which exhibited diverging Q^{rad} (Fig. 2A). In the particular band studied, a BIC protected by symmetry was fixed at the center of the Brillouin

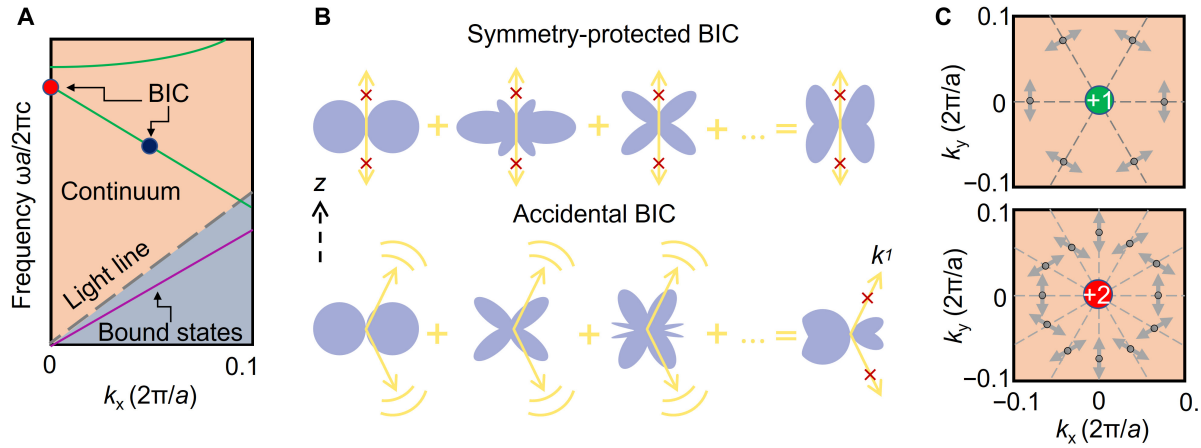

Fig. 1. Interpretation of BICs from multipolar analysis and topological charges. (A) Schematic of a typical dispersion diagram of PhCs. (B) BIC formation in terms of far-field multipolar analysis. (C) Schematic of topological charges characterized by polarization vector in the momentum space.

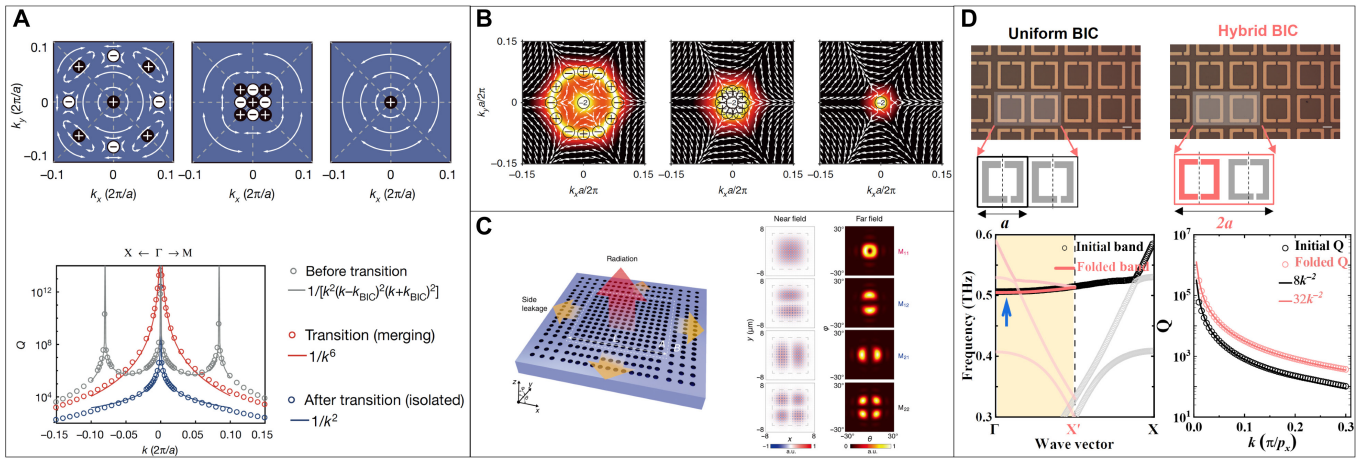

Fig. 2. Merging BICs and folded BICs to improve the quality factors in practice. (A) Dynamics of merging BIC in terms of topological charges by parameter tuning [28]. (B) Merging BICs with high-order topological charges [36]. (C) Miniaturized BICs with a heterostructure to confine photons in all the 3 dimensions [37]. (D) Hybrid BIC metasurfaces with mixed nonradiative BIC and quasi-BIC resonators [38]. a.u., arbitrary units.

zone, while the remaining 8 accidental BICs underwent evolution along the highly symmetric lines by continuously adjusting parameters such as the lattice period. All the BICs existed in the band protected by the nontrivial topological charges, and remained stable until the charges merged and annihilated into a single isolated BIC with a charge of +1 at the center of the Brillouin zone.

This merging process alters the intrinsic radiation behavior of an isolated BIC governed by the relation of $Q^{rad} \propto 1/k^2$ and additionally safeguards the radiation against scattering out of the cavity confined by the nearby accidental BICs (Fig. 2A). The topological property triggered a merging BIC, which complied with $Q^{rad} \propto 1/k^6$ and is very promising in suppressing the unexpected scattering losses due to fabrication defects or disorders and improving the upper limit of Q in practice. A record-high Q^{tot} of 4.9×10^5 was experimentally achieved by merging BICs, which was 12 times higher than the value of an isolated BIC. This milestone work could serve as the backbone in merging BICs to diverse more attractive studies.

To further explore the role of topological charges, high-order charges were studied in a hexagonal lattice PhC, which exhibited merging BICs at the Γ point with a topological charge of −2, as illustrated in Fig. 2B [36]. Moreover, a relation of merging BICs with a topological charge $q = \pm n$ could be generalized as $Q^{rad} \propto 1/k^{-2n-4}$. Another study demonstrated the confinement of light in all 3 dimensions by utilizing merging BICs that provided vertical confinement and photonic bandgap as mirrors for lateral confinement (Fig. 2C) [37], which has further improved the Q^{tot} to a higher value of 1.09×10^6. The lateral confinement also ensured a localized Bloch mode surrounded by the bandgap PhC, leading to a reduced modal volume of $V = 17.74(\lambda_0/n)^3$. The simultaneous increase in Q^{tot} and reduction of modal volume are expected to significantly enhance the Purcell effect, which would be beneficial for low-threshold lasers, chemical and biosensors, and nonlinear photonics [21].

The concept of merging BICs effectively increases the slope of Q^{rad} versus k (see bottom panel of Fig. 2A), which mitigates the impact of fabrication defects and disorders on Q^{rad} in practice. However, merging BICs have a stringent requirement of special band with multiple BICs in the momentum space and demand an extremely accurate design of resonators at subnanometer scale for the assembly of all the charges in the vicinity of Γ point. Recently, a generalized path was proposed to improve the lifetime and robustness of BICs with a hybrid BIC lattice. Different from conventional approaches to access quasi-BIC by breaking symmetry of resonators uniformly in a metamaterial lattice, the ability to selectively close radiative channels in the lattice as a whole allows for fine-tuning of the radiation density in the BIC and quasi-BIC hybrid lattice, as demonstrated in Fig. 2D [38]. This is a generalized approach that could be extended to any symmetry-protected BIC without requirements of accurate geometric design or band selectivity. The hybrid BIC lattice offers a strong and reliable way to achieve high-Q resonances that are more than 14.6 times greater than the conventional lattices. Such an advanced structure provides an excellent method for obtaining precise, high-Q resonances that are not affected by fabrication disorders, ultimately reducing the negative impact of common fabrication flaws on resonance quality. The process of band folding reveals the origin of the robust and high-Q resonances in the hybrid BIC lattice and uncovers multiple Fano resonances that arise from the otherwise bounded eigenstates at X, Y, and M points in the momentum space. The robust and high-Q multiple Fano resonances are especially important in the THz regime for pulse generation, sensing, and communications.

BICs of splitting topological charges

To study circularly polarized states stemming from BICs, the in-plane C_2 symmetry was first broken, leading to pairs of circularly polarized states (C points) generated from the symmetry-protected BICs (V points as vortex polarization singularities, as shown in Fig. 3A) [30]. A theoretical demonstration soon followed, showing that breaking the in-plane C_2 symmetry was not necessary for the emergence of C points, which could also appear near the K point and Dirac-degenerate points in a PhC with honeycomb lattice, with in-plane inversion symmetry and time-reversal symmetry conserved (Fig. 3B) [39]. In addition, the work pointed out that only a pair of C points with identical (opposite) handedness and opposite (identical) topological charges could be annihilated (merged) together. However, this method is not universal since the achievement of C points is reliant on the incompatible symmetry of BICs (a double-degenerate BIC). Generation

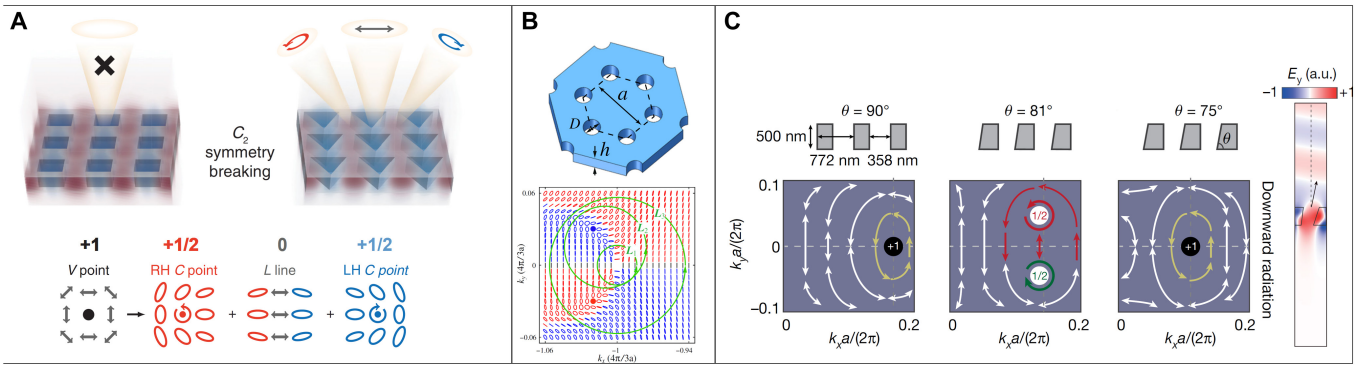

Fig. 3. Polarization manipulation and asymmetric radiation enabled by topological charge spitting. (A) Circular polarization radiation at Γ point by splitting topological charge (+1) in the process of symmetry breaking of a PhC with intrinsic chirality and (B) circular polarization radiation near K point and Dirac-degenerate points in a honeycomb lattice PhC [30,39]. (C) Unidirectional radiation by splitting topological charge with slant geometry by breaking up-down symmetry (*z*-axis) [43].

and annihilation of BICs and *C* points were also probed with higher-order topological charges (−2) by breaking the C_6 symmetry. Two merging processes of *C* points were observed by breaking the up-down symmetry, where unidirectional radiative resonances with leaky channels of drastically different radiative lifetimes emerge [40]. Without breaking the up-down symmetry, the *C* points would not appear at Γ points, and circularly polarized radiation could not be measured at normal incidence. However, they could still be accessed at other points in the band, which is known as extrinsic chirality [41,42].

When the up-down symmetry was broken, the first experimental demonstration of unidirectional radiation was realized in a 1-dimensional silicon PhC slab with slant sidewalls as shown in Fig. 3C. A transverse electric (TE-like) band was found to have an accidental BIC at off-Γ point in the reciprocal space that possesses $q = +1$ when the in-plane mirror symmetry and out-of-plane (*z*-axis) symmetry is conserved [43]. When the out-of-plane symmetry was preserved, the radiation properties were the same along the $+z$ and $-z$ directions. However, when the symmetry was broken by tilting the sidewalls of the grating along the *z*-direction, the radiation symmetry was also broken, resulting in the splitting of the +1 charge into paired half-integer charges. These charges were protected by the symmetry along the *y*-axis (Fig. 3C). At the same time, BIC disappeared and the radiation decay rates toward $+z$ and $-z$ directions decoupled for the 2 half-integer charges whose radiation was circularly polarized with opposite helicities. By continuously tuning the tilting angle of the slant sidewalls, the 2 half-integer charges merged into an integer charge for the downward radiation forming an accidental BIC again, but the radiation channel along the upward direction was still open. This specific profile enabled an ideal asymmetric unidirectional emission with measured asymmetric ratio as high as 27.7 dB and Q^{tot} of 1.6×10^5.

Emerging mechanisms and applications of BICs

Radiation is a ubiquitous phenomenon to bring non-Hermicity to photonic systems, so that a topologically robust high-*Q* resonance paves the way to understand the intrinsic physics underneath the general system. The higher *Q* led to a promising platform to enhance light–matter interactions in topological photonics, which is beneficial to polish the performance in topologically integrated optoelectronic devices [44]. Merging BICs also provide alternative methods for realizing large-area lasers combined with optical cavities, modulating light radiation using active media, and generating new frequency components through nonlinear effects. Recently, interesting mechanisms of BICs integrating with topological photonics and flat band were reported, and applications in wavefront manipulation were introduced with nonlocal metasurfaces.

Topological and flat-band BICs

One of the most canonical behaviors in topological photonics is the support of the topologically protected edge states confined on the interface between topologically trivial and nontrivial PhCs [45,46]. In 2015, an all-dielectric photonic system was proposed to exhibit a pair of spin-locking edge states within the bandgap analogous to quantum spin Hall effect [47]. This type of edge states mainly exists in the vicinity of Γ point and above the light cone, which provides a potential condition to investigate the interactions between BICs and edge states. In addition to the bound topological edge states in the continuum explored in 2021 (Fig. 4A) [48], another method to combine BICs with topological flat bands was proposed by extending the flat band enabled by bilayer honeycomb PhC at a magic angle into the continuum as shown in Fig. 4B [49]. The band with a BIC at Γ point could be folded and forms a flat band under the appropriate twist angles and spatial distance of 2 identical PhC slabs. This work provides an adjustable way to trigger a high-*Q* quasi-BIC by introducing one more flexible degree of freedom, removing the requirements of geometric symmetry-broken or the precise incident angles. To explore greater dimensions, Floquet edge states [50,51] and corner states in high-order topological insulators [52–54] were also studied to analyze the connection between topology and BICs.

Topological BICs not only inherit the intrinsic properties originated from dispersion relationship in topological systems but also provide additional radiation properties toward free space. Topological BICs paved a feasible way to couple and radiate topological edge states to free space, which omits the complicated coupling channels in topologically integrated chips. In addition, flat band and flexibly adjustable *Q* are beneficial to second-harmonic generation (SHG) in nonlinear materials on which the incident angle of pump light exerts a negligible impact. To date, topological photonics has combined with nonlinearity [55,56], non-Hermicity [57,58], and synthetic dimensions [59] to explore topological properties in multiple degrees of freedom and thus exhibits a plethora of scenarios to investigate the physics of BICs. The combination of topologically protected edge

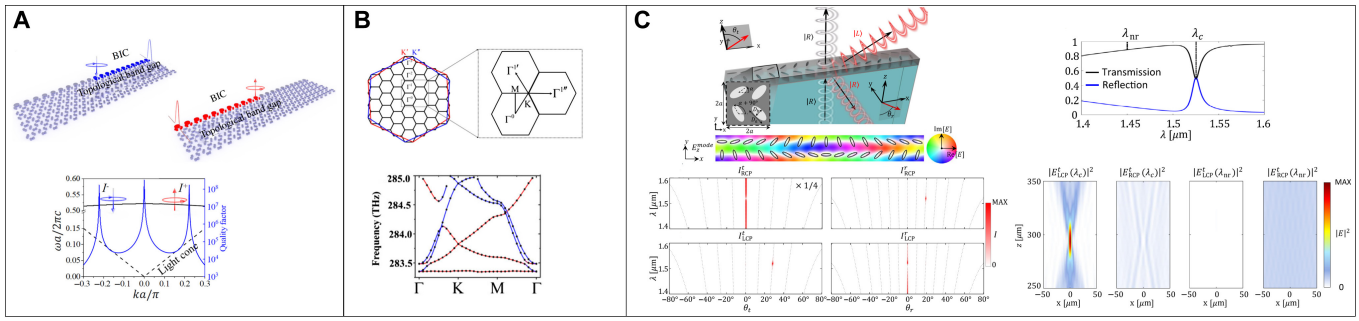

Fig. 4. BICs enabled by different physics and their applications. (A) Bound topological edge states in the continuum [48]. (B) Flat-band BICs [49]. (C) Application of narrow-band BICs in nonlocal metasurfaces [76].

states and BICs guaranteed both lateral and vertical confinement and would lead to more tight mode localization with further reduced radiative losses [37]. Another interesting combination lies at exploring BIC-supported zero-index media in PhCs by designing a Dirac cone at Γ point in the band structure [60,61]. Such a combination could enable longer coherence length with low losses and benefit linear and nonlinear optics in a large-area medium.

Applications of BIC in nonlocal metasurfaces

Manipulation of wavefront can be achieved through metasurfaces, which can be classified into 2 types: local and nonlocal metasurfaces. Local metasurfaces engineer the wavefront by individually manipulating each unit cell [62–64], whereas nonlocal metasurfaces support resonant modes spatially extending across adjacent unit cells that are formed by collective excitation [65–67]. BICs and quasi-BICs (manifesting as Fano resonances) are typically induced in nonlocal metasurfaces. Although local metasurfaces have revealed extraordinary capability to shape the wavefront, they commonly lack spectral selectivity [62,68–70]. In contrast, nonlocal metasurfaces offer great spectral selectivity with a narrow linewidth [71,72]. In the past few years, nonlocal metasurfaces have been widely applied in sensing [24,25], optical signal processing [72], augmented reality [73], and harmonics generation [74,75]. However, traditional nonlocal metasurfaces have limited capabilities in tailoring wavefront.

Simultaneous manipulation of light in both spatial and spectral domains was realized with nonlocal metasurfaces supporting BICs, as shown in Fig. 4C [76,77]. Symmetry-protected BICs were utilized to achieve frequency selectivity and introduce a geometric phase that operates only within the spectral range of the quasi-BIC resonances. The Pancharatnam–Berry (P-B) phase enables additional phase of 4α (α is orientation angle of dimers) for the transmitted left-handed circular polarization (LCP) and reflected right-handed circular polarization (RCP) with RCP incidence, while the phases of reflected LCP and transmitted RCP are invariant to α. Therefore, any phase profile is feasible to engineer the wavefront in the spectral vicinity of quasi-BICs. Note that the electric field of nonlocal metasurfaces exhibited a collective supermode (Fig. 4C), and the nearest-neighbor coupling led to a blueshift of resonance from the eigenvalue of isolated resonators in the nonlocal metasurfaces. Consequently, the deflection only occurred at a narrow wavelength range of BICs, leaving the remaining spectrum transparent without wavefront distortion. Nonlocal metasurfaces also enable approaches to control more modes simultaneously [67].

Light focusing of nonlocal metasurfaces to function as metalenses is feasible with larger numerical aperture (NA) as well as narrow linewidth. For nonlocal metalenses, NA can be described by: $NA^2 \leq \frac{\omega_0 / k_0^2}{|b|Q}$, where b is a constant, Q is quality factor, k_0 is the free space wave vector, and ω_0 is the angular frequency of the mode at $k = 0$. A flat band ($|b|$ is small) would compensate the high-Q resonance and offer a high NA [76,78]. Based on the idea of nonlocal metasurfaces, researchers have demonstrated the creation of multifunctional metalenses that can modulate resonant wavelength, Q factor, dispersion, and wavefront at multiple wavelengths. This was achieved by cascading nonlocal metasurfaces, while maintaining transparency for all other wavelengths [79]. The nonlocal BIC metasurfaces hold great promise for augmented reality glasses as a beam splitter with the capability to control wavefront at selected frequencies (i.e., colors) while remaining transparent at off-resonance frequencies [73,80].

In addition to the full control of wavefront of coherent light, partially coherent radiation from thermally emitted light could be manipulated by nonlocal BIC metasurfaces [81]. The thermal metasurfaces that could radiate with selected wavefronts, controllable linewidth, spin and angular orbital moments, and coherence were demonstrated. Nonlocal BIC metasurfaces would enrich applications in wavefront selection [82], quantum optics [83], and nonlinear optics [84,85]. It should be noted that efficiency remains a common challenge for both local and nonlocal metasurfaces, with a theoretical limitation of 25%. However, chiral BIC metasurfaces (see Applications) have shown the potential to overcome this limitation, achieving unlimited efficiency of up to 100% [86].

Applications

Chiral light and vortex beam generation

Chirality, as a fundamental feature of nature, refers to the geometric attribute of objects that does not coincide with their mirror images [87,88]. Metamaterials composed of chiral elements exhibit strong chiroptical responses [89], which have been demonstrated by metamaterials with helices [90,91], N-shaped structures [92–94], and multilayered structures [95–97]. However, achieving efficient and high-Q chiroptical effects remains a challenge, which leads to the limited ability in chiral emission [98], circular polarization-sensitive photodetection [99], and chiral molecular separation [100] due to weak chiral light–matter interactions.

Consistent with the generation of circularly polarized states by topological charge splitting, intrinsic chirality was explored under BIC schemes. Maximal chirality could be reached by utilizing dimers composed of classical dielectric elliptical bars with symmetry-protected BICs, which could be numerically analyzed with coupled-mode theory (Fig. 5A) [101]. Achieving optimal chirality requires precise control over the radiation coupling of eigenstates to free space, and BICs provide an ideal starting point for analysis as they are fully decoupled from free space at their initial state. By breaking C_2 symmetry with an increase of θ, BICs were transformed into quasi-BICs, but the overall structure remained intrinsically achiral with merely in-plane symmetry broken. Out-of-plane symmetry was further broken by introducing a vertical offset (d) of the elliptical bars, which eliminated the mirror symmetry, and thus intrinsic chirality emerged. By adjusting the parameters θ and d, the dissipation matching condition could be satisfied in the critical coupling regime, allowing for the achievement of maximal chirality. In addition to breaking symmetry by tuning parameters θ and d, chiral quasi-BICs were also systematically studied with double-layer metasurfaces [86], and maximal chirality could be achieved by adjusting the orientation angles (α) of elliptical bars and the relative rotation ($\Delta\alpha$) between the up-down bars in the 2 layers of metasurfaces (Fig. 5B). Additionally, the adjustable parameters provide freedom to freely control the radiation phase and guaranteed maximal transmission amplitude. BICs enable highly efficient wavefront shaping of circularly polarized light and sharp frequency selectivity. The utilization of BICs provides a promising approach to surpass the traditional 25% efficiency restriction in conventional planar metasurfaces under linear polarization illumination [76]. However, breaking the up-down symmetry of intrinsic chirality required to implement these designs is currently only possible in the microwave range, where 3-dimensional samples are more easily accessible [102]. Implementing these designs in the infrared and visible ranges remains challenging due to fabrication difficulties. One solution was reported with PhCs of slant sidewalls breaking both in-plane and out-of-plane symmetries at visible frequencies [103], which enabled that chiral emission with giant field enhancement and a small divergent angles were experimentally observed (Fig. 5C) [98]. Although fabrication in nanoscale is challenging, multistep fabrication solutions were proposed for dielectric dimers with arbitrary height difference [104]. This approach would remove the fabrication barrier of breaking the up-down symmetry in PhCs, enabling the experimental exploration of more intriguing phenomena in shorter wavelengths. Most recently, planar dielectric metasurfaces were reported with optimized efficiency of circularly polarization conversion and very narrow spectral linewidth empowered by BICs without breaking out-of-plane symmetries [105]. Similar to chirality, the absorption of circularly polarized light was studied on the basis of BICs with a stereoscopic split ring resonator array covered by metals on the surface in THz regime [106].

One more intriguing aspect of BICs is their ability of light manipulation through spin Hall effect with circularly polarized light [107]. The strong spin–orbit interactions are enhanced by the topological vortices around BICs, where wave vector-dependent P-B phase gradient and conventional P-B phase gradient of cross-polarized light lead to the synthesized spin-dependent lateral light shifts. Vortex beam is another important consequence of topological charges of BICs in radiation [29]. Early in 2011, vortex beams with quantum numbers of optical

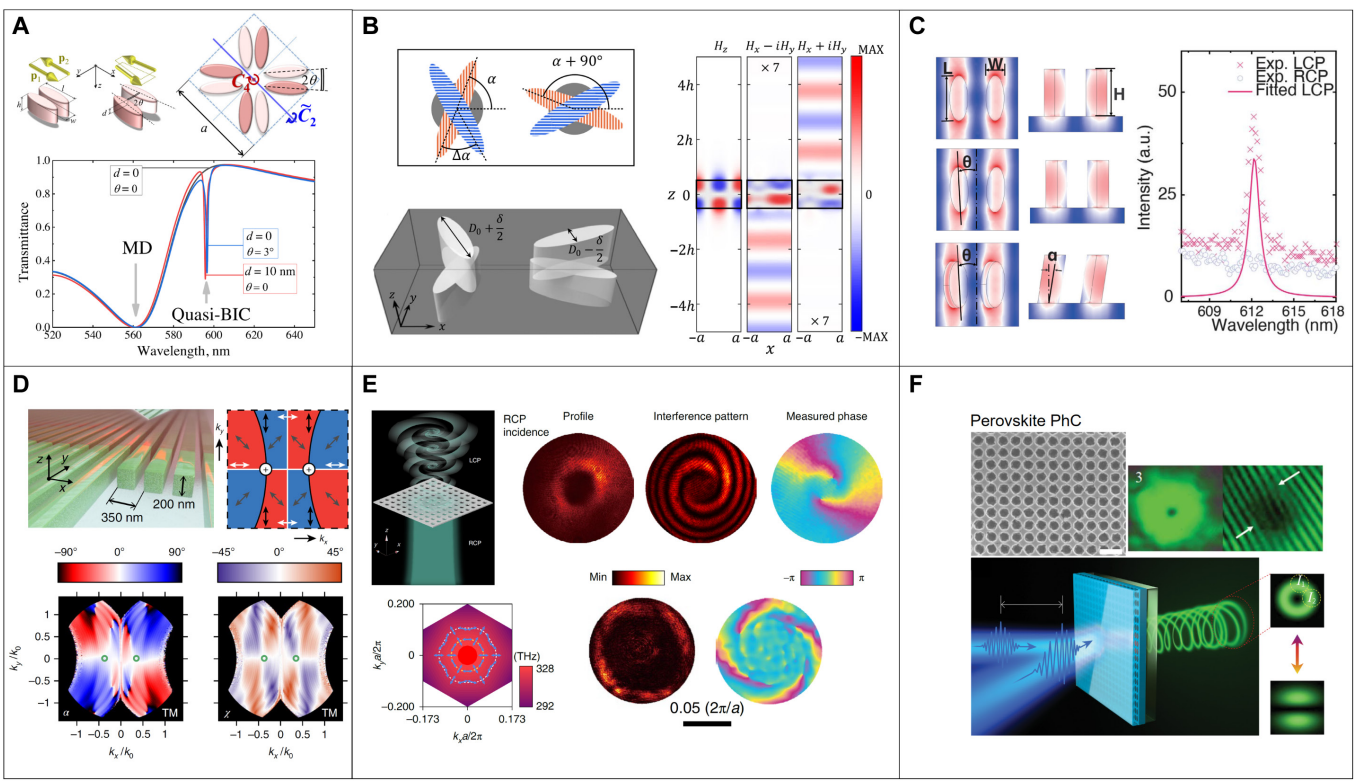

Fig. 5. Applications of BICs in intrinsic chirality and vortex beam generation. (A) Chiral BIC metasurfaces with a maximal circular dichroism [101]. (B) Chiral BIC metasurfaces supporting high-efficiency wavefront shaping [86]. (C) Chiral emission from a BIC metasurface with slant sidewalls [98]. (D) Experimental observation of polarization vortex from BICs [29]. (E) Vortex beam generation via momentum-space polarization vortices centered at a BIC [109]. (F) Vortex lasing based on a perovskite PhC [18].

angular moment l =1, 2, and 3 were demonstrated using PhCs at Γ point, which possessed topological charges of $q = 1, 2$, and 3 [108]. Interpreted from BICs, it is anticipated that the light radiated by modes around BICs would display a vortex in the far-field polarization profile. The first experimental observation of full polarization states around a BIC was reported in [29] demonstrating the presence of topological vortex as shown in Fig. 5D. Characterized by polarization ellipse, the vortex exists not only in polarization angle (α) but also in ellipticity (χ). Similar to the multipolar analysis, BICs in the grating can be explained as a Friedrich–Wintgen bound state arising from the interference between 2 resonant dipolar contributions (z-oriented electric and y-oriented magnetic dipoles). Based on the strong polarization anisotropy in the vicinity of BICs in momentum space of a PhC, P-B phase will be added to cross-polarized radiation with a circularly polarized incidence. Different $\boldsymbol{k}$ components of incidence would interact with guided resonances with the in-plane wave vector $\mathbf{k}_{||}$, and the transmitted cross-polarized radiation would automatically possess a spiral phase front with an optical angular momentum (topological charge) $l = \mp 2 \times q$ where q is the polarization charge of BICs and $\mp$ is for RCP and LCP incidence, respectively (Fig. 5E) [109]. The generated vortex is a high-order quasi-Bessel beam that is diffraction resistant, and the PhC has no structural center, making it free from alignment. Higher orders of orbital angular momentum can be easily accessed by using samples of higher symmetry or by tuning the working wavelength. Beyond passive devices, the generation of vortex beam in radiation is also feasible in cavities with active media. Under the similar interpretation of topological charge of BICs, vortex lasing was reported in a microlaser based on a lead bromide perovskite PhC (Fig. 5F) [18]. Furthermore, BIC condition could be broken by introducing imaginary part in the cavity in an ultrafast scale (1 to 1.5 ps), and thus, ultrafast switching of the polarization from vortex to linearly polarized beam was demonstrated with ultralow energy consumption.

Nonlinear optical frequency conversion

BICs have received great attention in the field of nonlinear frequency conversion. A plethora of interesting PhCs and metamaterials based on BICs or quasi-BICs have opened up a new path to boost harmonics generation with high yield and efficiency owing to high Q and extreme local field enhancement. Nonlinear optical processes at nanoscales, such as second-, third- and high-harmonic generation, THz generation, and frequency mixing effects, have attracted significant interest in both scientific and industrial developments for high conversion efficiency and miniaturized devices. Regarding nonlinear effects in conventional bulky media, optical pump of high intensity is typically required to observe harmonics given the inherently weak nonlinear interactions, and complex phase matching between the fundamental and harmonics is essential. By contrast, metamaterials and PhCs relax the strict phase-matching conditions and enhance local fields in a tight volume [110,111]. In this section, we review recent advances in nonlinear optical frequency conversion with BIC metasurfaces.

SHG

SHG relies on the second-order nonlinear susceptibility of crystals, which only occurs in noncentrosymmetric crystalline structures, and thus, the studies mostly concentrated on III-V semiconductors materials with high second-order coefficients, such as AlGaAs [74,112–115], GaP [116,117], and GaAs [118,119]. Recently, an isolated AlGaAs resonator was reported to support a quasi-BIC interpreted from multipolar analysis, and further reduction of radiative losses was realized by optimizing the substrate configuration with an epsilon-near-zero layer (Fig. 6A). The high-Q quasi-BIC enabled an experimental observation of SHG efficiency as high as 1.3×10^{-6} W^{-1}, which was more than 2 orders of magnitude higher than other types of resonances [74]. With a metasurface array of AlGaAs resonators, SHG efficiency could theoretically be boosted up to 10% at a moderate pump intensity of 5 MW/cm^2 with a symmetry-protected quasi-BIC that exhibits 6 orders of magnitude higher than magnetic dipole resonances [115].

Early in 2018, Fano resonances rooting in symmetry-protected BICs revealed a great improvement of SHG with a symmetry-broken L-shaped GaAs metasurface compared with the symmetry-conserved nanodisk GaAs slabs [119]. Metasurfaces composed of dimers of elliptical cylinders were also probed with symmetry-protected BICs to boost the SHG on a GaP material platform, which offered a relatively high nonlinearity, high refractive index, and low loss. The SHG efficiency of 0.1% W^{-1} was achieved with 100-times lower intensities of pulsed pump (10 MW/cm^2) compared with previous reports in the literature. Additionally, efficient SHG was demonstrated on this platform with a conversion efficiency of 5×10^{-5}% W^{-1} pumped at the central wavelength of the quasi-BIC resonance with a continuous wave intensity of 1 kW/cm^2 (Fig. 6B) [116].

Low-index materials, such as lithium niobate (LN), have large second-order nonlinear susceptibilities and transparent window from ultraviolet to infrared [120], which are promising for SHG despite the difficulty in accurate fabrication. Although deep etch of LN with an accurate geometry is challenging, shallow etch would enable flexible engineering of the abundant modes in PhCs and induce high-Q BICs. Initiated from the guided resonances in the unpatterned LN slab, an accidental BIC was observed by the interference between TE and transverse magnetic (TM) modes in the shallow-etched LN metasurface which would significantly boost the SHG emission [121]. Experimental demonstration of enhanced SHG boosted by symmetry-protected BICs was reported in [122] as shown in Fig. 6C. Shallow-etched z-cut LN metasurfaces were probed to utilize the largest nonlinear susceptibility, and SHG was enhanced by TM modes. More recently, hexagonal boron nitride metasurfaces made of low-index materials were used for SHG covering the whole visible spectrum, hosting symmetry-broken BICs with an enhancement factor above 10^2 [123]. SHG is commonly probed in materials without centrosymmetry, and second-order nonlinear optical responses are not allowed in the bulk with centrosymmetry such as silicon and germanium. Nevertheless, the surface has no centrosymmetry and is accessible to SHG. Taking advantage of BICs to strengthen the local fields, efficient SHG in a symmetry-broken silicon metasurface was experimentally observed with an efficiency of 1.8×10^{-4} W^{-1} [124].

High-order harmonic generation and frequency mixing

Third-harmonic generation and high-order harmonic generation at nanoscales with quasi-BICs have mainly concentrated on silicon-based nanostructures [75,125–129]. Based on quasi-BICs in an isolated silicon nanoparticle similar to [74], high-order harmonics including the third and fifth harmonics were obtained [126]. In a symmetry-protected BIC metasurface in the mid-IR regime, odd harmonics up to the 11th order were

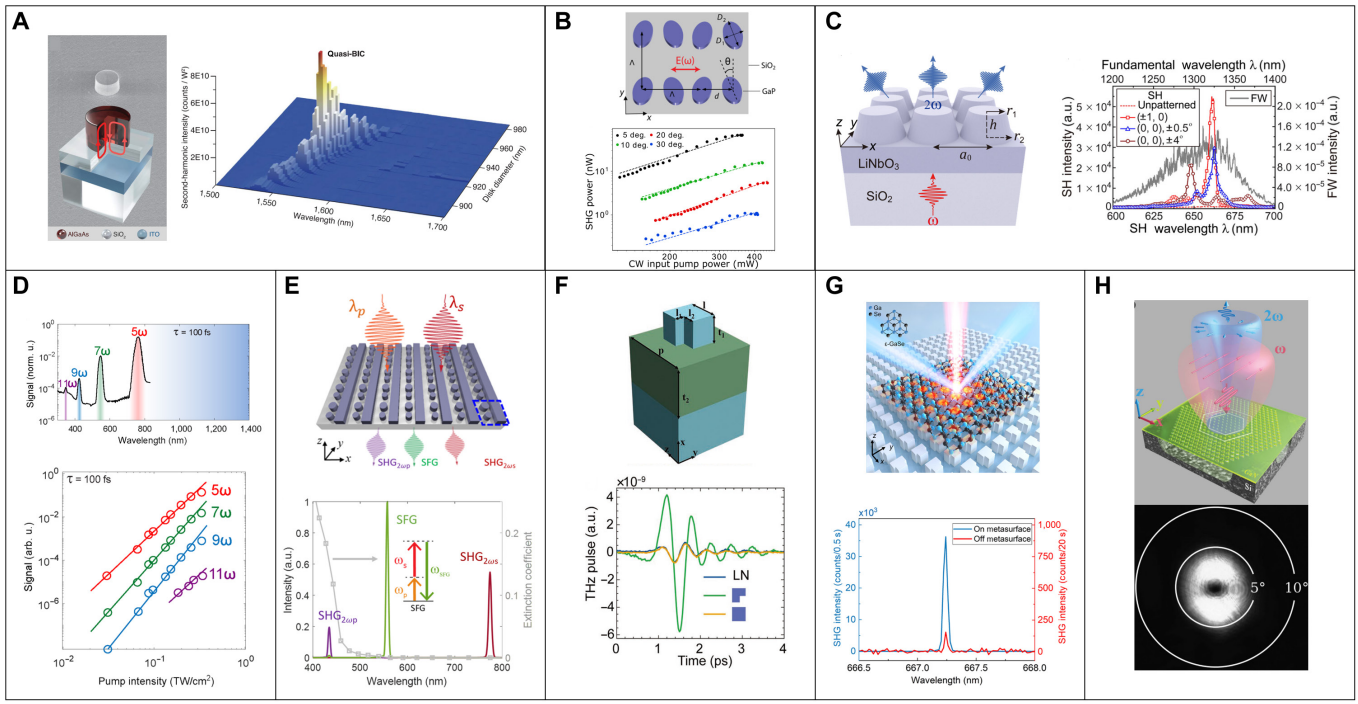

Fig. 6. Applications of BIC in nonlinear metasurfaces. Efficient SHG in (A) an isolated AlGaAs resonator [74], (B) GaP [116], and (C) LN metasurfaces supporting BICs [122]. (D) Third-harmonic generation and high-order harmonic generation in an isolated silicon nanoparticle supporting BICs [125]. CW, continuous wave. (E) SFG in GaP metasurfaces boosted by BICs [130]. (F) Single-cycle THz generation in LN metasurfaces enhanced by BICs [131]. (G) SHG enhancement in a hybrid BIC metasurface integrated with few-layer GaSe [136]. (H) Vortex beam of SHG in a GaN PhC empowered by BICs [142]. CW, continuous wave.

observed, and the transition from perturbative to nonperturbative regimes was traced as shown Fig. 6D [125].

Moreover, there are also intricate frequency mixing phenomena at the nanoscales that involve at least 2 frequencies, such as sum frequency generation (SFG), four wave mixing, and difference frequency generation (DFG). Highly efficient SFG was probed with high-Q metasurfaces empowered by BICs in the material platform of GaP (Fig. 6E) [130]. Illuminated by pump beam at 875 and 1,545 nm, a normalized conversion efficiency of 2.5×10^{-4} W^{-1} was obtained for SFG in the visible. Different from harmonic generation, the maximal efficiency of SFG was measured for inputs of nonparallel polarization. Similarly, DFG could also be enhanced by BICs and the resultant longer wavelength signals, e.g., THz emission, could enable compact light sources [131,132]. With giant second-order sheet nonlinear susceptibility, single-cycle THz emission has been fully explored in metallic metasurfaces enhanced by magnetic-dipole resonances [133–135]. However, the large ohmic loss, low damage threshold, and small interaction volume of plasmonic resonators hinder the nonlinear conversion efficiency in metallic resonators. Dielectric metasurfaces would avoid all the abovementioned shortcomings, and efficient THz pulse emission boosted by BICs was recently reported based on LN platform. Localized field enhancement in LN film was obtained by the patterned SiO_2 metasurface due to the relatively lower index of SiO_2, and 17 times improvement of THz emission at 0.7 THz in contrast to the unpatterned LN thin film was experimentally observed as shown in Fig. 6F [131].

Hybrid and functional nonlinear metasurfaces

2D materials such as transition metal dichalcogenides and gallium monochalcogenides have been revealed as excellent nonlinear optical materials with giant nonlinear susceptibilities. However, the short interaction length with light limits their nonlinear responses. The solution was raised by integrating the thin films with high-Q resonators, and hybrid metasurfaces supporting BICs enable an excellent approach for enhancing interactions with 2D materials [136–141]. Few-layer gallium selenide (GaSe) is a typical example that exhibits giant second-order nonlinear susceptibility of ~1,700 pmV^{-1} at telecom band [136]. Boosted by silicon-based metasurfaces supporting symmetry-protected BICs, the hybrid GaSe-metasurface revealed a 9,400-fold improvement of SHG compared with a bare GaSe flake (Fig. 6G) [136].

Functional nonlinear metasurfaces integrating harmonics generators and manipulators would further enrich the potential applications in which phase, amplitude, polarization, and radiation direction of harmonics were finely controlled [142–146]. Asymmetric radiation is an interesting topic both in linear and nonlinear regimes [43,143,147]. In nonlinear regime, asymmetry radiation of SHG in the forward and backward directions was theoretically proposed in a bianisotropic metasurface supporting quasi-BICs [143]. Highly normal-direction concentrated vortex beam was observed in the SHG based on a GaN PhC that supports doubly resonant BICs (Fig. 6H) [142]. The great enhancement of SHG by the high-Q resonances led to a conversion efficiency of 2.4×10^{-2} W^{-1} under continuous wave excitation. With the giant enhancement of harmonics generation, dynamical control of wavefront of harmonics was feasible via tuning polarization and wavelength [145].

Boosted by BICs in metasurfaces, it is expected to enhance the nonlinear responses; however, accurate fabrication of nanostructures remains a challenge for certain materials despite the advanced fabrication technologies of silicon. Factors that need to be considered in the fabrication process include geometry,

simplicity of fabrication, surface roughness, and others [148]. For interesting materials without appropriate fabrication approach, an alternative solution is to excite BICs in a metasurface with a low-index material so that the mode is largely confined in the high-index nonlinear materials to boost light–matter interactions [149,150].

Sensors

With the goal of miniaturization and improved sensing performance, highly sensitive sensors that can be integrated onto a chip with ease of use, good portability, and free from maintenance, have become increasingly important [1]. The unique characteristics of symmetry-protected BICs, such as narrow linewidth, wide frequency scalability, and a well-defined spectrum over a broad wavelength range, provides a promising platform for sensing technology, particularly for imaging-based molecular barcoding in a pixelated configuration (Fig. 7A) [24]. Absorption signatures of various molecules could be mapped in the spectra constituted by a series of quasi-BICs, each of which was linearly encoded to spatial location of the pixels. The BIC-based molecular barcoding provides more sensitive detection of molecular fingerprints with spectral resolution determined by linewidth of quasi-BICs. In this configuration, vibrational information of analyte could also be readout for chemical identification and compositional analysis. Similar BIC configuration was adopted to develop a 1-shot imaging-based optical data acquisition and processing method, as shown in Fig. 7B [26]. An ultrasensitive label-free biosensing platform was demonstrated by combining the pixelated BIC metasurfaces with a commercial complementary metal oxide semiconductor camera, capable of sensing less than 3 molecules/μm^2. The hyperspectral decoder approach correlated spectral information with spatial index of complementary metal oxide semiconductor pixels, allowing high-resolution spectral information to be extracted from a 1-shot image at a fixed wavelength. This is a wise spectrum-extraction scheme to eliminate the need for the bulky and expensive spectrum instrumentation. Integrating the pixelated metasurface chip with optofluidic system enabled more flexible and real-time detection of biomolecules. The reported sensitivity of 701/RIU and 0.41 nanoparticle/μm^2 for detecting a 204 fM solution demonstrated the potential of this approach in detecting breast cancer extracellular vesicles encompassing exosomes. In addition to continuously tuning the central wavelength of symmetry-protected BICs in parameter space at normal incidence, similar modulation could also be accessible in momentum space by continuously tuning the incident angles (Fig. 7C) [25]. The type of angle-multiplexed BIC spectra delivered a larger number of resonances (more than 200 resonances) from a single metasurface chip than those in geometry parameter space, which were limited only by the instrumental angular resolution (1.4 cm^{-1} spectral step size) and range of incidence angles (13° to 60°). A similar mechanism used in [24] was applied to capture the molecular absorption fingerprint with high sensitivity (0.27 pg/mm^2) and chemical specificity.

A high-Q resonance with narrow linewidth is essential for a good sensor to clearly resolve the spectrum caused by analyte, and the near-field interactions with the analytes can significantly influence overall sensitivity. Plasmonic sensors have been adopted to enhance the local field within the subwavelength scale, but they typically feature low-Q resonances around 10 due to the intrinsic losses in metals [151–153]. Empowered by symmetry-protected BICs, a plasmonic nanofin metasurface was reported with Q up to 180, as shown in Fig. 7D [151]. Quasi-BICs were realized by breaking the out-of-plane symmetry of the nanofins via introducing a slanted sidewall with an angle α fabricated by 3D laser nanoprinting, and the nanofin transformed from a rod to a triangular-type structure. Radiative losses could be tailored by adjusting the angle α, and the coupling regime of the cavity could then be tuned to cross the undercoupling, critical coupling, and overcoupling regimes. In this work, a similar pixelated metasurface taking advantages of the broad wavelength coverage of BICs was developed for molecular sensors. Interestingly, different types of modulation in the spectra of the pixelated metasurface occurred, dominated by the coupling regimes of the resonators. Instead of metallic metasurfaces, applications of BICs in dielectric resonators would reduce ohmic losses, further improving the overall Q of resonances and thus a better sensitivity. A sensitivity of 178 nm/RIU was reported in a dielectric metasurface supporting a quasi-BIC with Q of 2,000 in the visible and infrared regimes [154]. Ultralow molecular weight detection of 186 Da was demonstrated with a 6-nm spectral shift per less than a 1-nm-thick

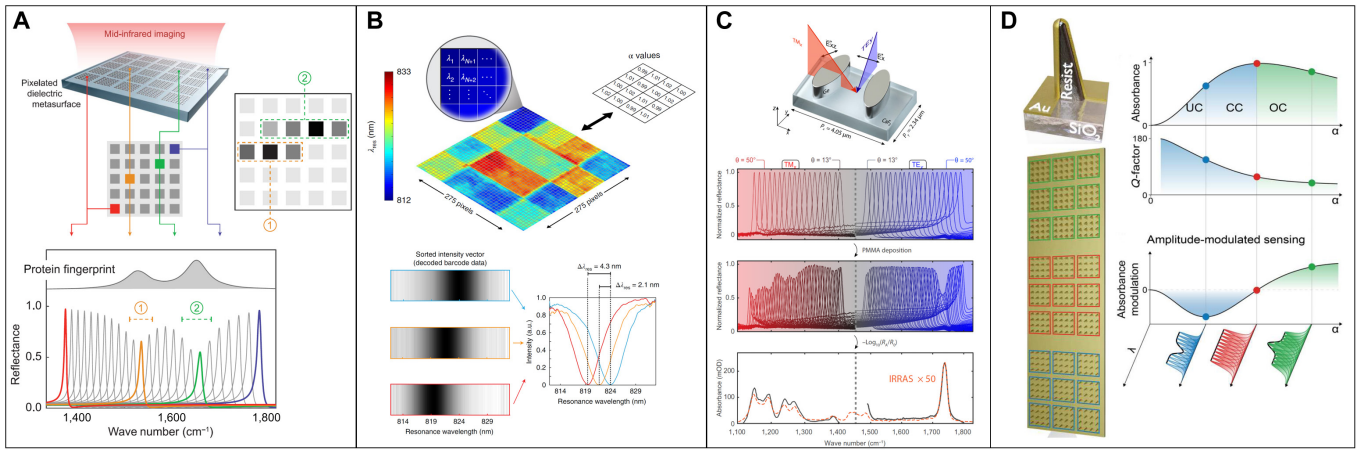

Fig. 7. Applications of BIC in sensors. (A) Imaging-based molecular barcoding with a pixelated BIC metasurface [24]. (B) Hyperspectral imaging and biodetection enabled by BIC metasurfaces [26]. (C) Broadband molecular fingerprint retrieval with an angle-multiplexed BIC metasurface [25]. (D) A BIC-enhanced senor with a plasmonic metasurface to further enhance local fields [151].

single molecular layer, showing the excellent sensing performance of BIC-based sensors. Sensors based on symmetry-protected BICs have also been reported in THz regime [155] and applied to enhance the fluorescence emission and Raman scattering [156].

Nanolasers

The future of information processing is likely to involve photonic integrated circuits compatible of parallel signal processing, with nanolasers as the most critical integrated components [17]. Highly efficient room-temperature nanolasers that feature a compact cavity and broad wavelength selectivity are in high demand for various applications, including biological imaging, near-field sensing, integrated photonics, adjustable light sources, and cutting-edge display technologies [157,158]. Recent developments of BIC physics enable new strategies to access long-lived and spatially confined resonances that offer precise manipulation of far-field lasing radiation.

Early in 2017, a single-mode lasing action based on BICs in PhCs was reported at room temperature consisting of several $In_xGa_{1-x}As_yP_{1-y}$ multiple quantum wells that operated around the telecommunication wavelength [19]. The intrinsically infinite Q of a BIC ensured that lasing could occur in arrays as small as 8 × 8 resonators. Typically, the smaller size of a BIC cavity leads to a rapid decrease in Q. However, merging BICs can slow down this trend, ensuring a high-Q resonance even in a cavity with smaller footprint. The idea was applied in a nanolaser based on an infinite-size InGaAsP PhC slab as shown in Fig. 8 [21]. Lasing threshold was found to be 1.47 kW/cm^2 that is much lower than other BIC-based lasers. Mode sizes also decreased at merging BIC states, and the far-field radiation patterns revealed a clear shrink until the merging state at a = 574 nm.

A comprehensive investigation of lasing operation based on BIC metasurfaces was presented in [22]. The results showcased the use of symmetry-protected BICs for low-threshold lasing (1.25 nJ) with a high spontaneous emission coupling factor of 0.9, while maintaining a high-Q resonance. In addition to low-threshold lasing, directional lasing is another key factor [20,34]. Although subwavelength PhCs do not naturally permit radiation at BICs, it is possible to create controllable leaky channels by altering the period of the array, thereby adjusting the diffraction orders (Fig. 8B) [20]. High Q could be sustained even when certain leaky channels were open, and excellent directivity with tunable lasing angles covering 0° to 25° could be achieved, as demonstrated in a GaAs nanopillar array.

With the ability to control lasing threshold and directivity, BIC mechanisms also offer the potential for manipulating lasing polarization and wavefront. For instance, BICs have been shown to generate vortex beams, which have unique characteristics of hollowness, diffraction resistance, and quantized orbital angular momentum. By integrating BICs with active media, e.g., InGaAsP multiple quantum wells, coherent vortex beams have been generated, with the lasing direction of the vortex beams controlled by adjusting the symmetry of resonators (Fig. 8C) [159]. In addition, ultrafast control of lasing polarization between vortex and linearly polarized beams was demonstrated in perovskite-based microlasers [18]. As discussed in the section of chiral light generation, another polarization state, circular polarization, can also be derived from BICs, and intrinsic chirality spawned from up-down symmetry breaking. Chiral quasi-BICs were demonstrated with high Q [98,103], and chiral lasing with LCP emission was observed at 612 nm with a threshold of 22.14 mJ/cm^2 (Fig. 8D).

Lasing based on various types of hybrid PhCs has been reported, such as CdSe/CdZnS core–shell nanoplatelets in the visible range [160]. Incorporating with high-Q resonances of PhCs, dramatic spectral and divergence angle enhancement of lasing was demonstrated from a 100-nm-thick organic molecule solution, resulting in significantly reduced threshold [161]. Meanwhile, BICs were characterized by their narrow spectral linewidths, making them highly sensitive to changes in refractive index and ideal for use as sensors. Nanolaser-based sensors not only offer coherent radiation but also exhibit exceptional sensing capabilities [162].

Perspective on THz Applications and Conclusion

THz radiation has exhibited great potential in applications of ultrafast dynamics, biomedical diagnostics, security inspection, wireless communications, and imaging [163–165]. The capabilities of nondestructive imaging and label-free sensing become the unique features of THz waves due to the deep penetration, low photon energy, and abundant spectral fingerprints of biomolecules [166,167]. With the large bandwidth and abundant spectral resources, THz band is increasingly recognized as a carrier frequency for the next-generation wireless communications. However, these promising applications still confront challenges from miniaturized and high-power sources, detectors with higher responsivities, modulators with low-power consumption and higher efficiency, switches with faster response and lower threshold, sensors with higher sensitivity

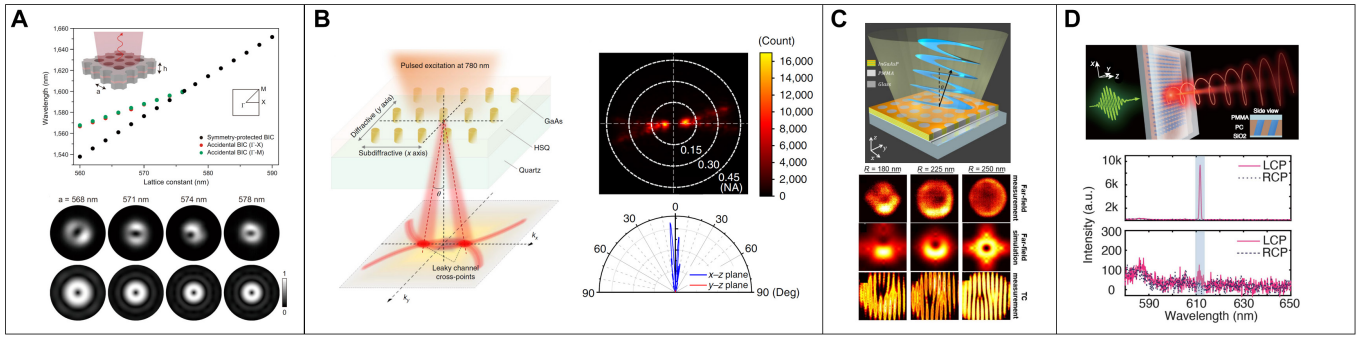

Fig. 8. Applications of BICs in lasing. (A) A nanolaser with ultralow-threshold and reduced mode volume empowered by merging BICs [21]. The directivity of nanolasers controlled by altering (B) the period of the arrays [20] and (C) the symmetry of PhCs [159]. PMMA, polymethyl methacrylate; TC, topological charge. (D) Chiral lasing with LCP emission achieved by breaking up-down symmetry of PhCs [98].

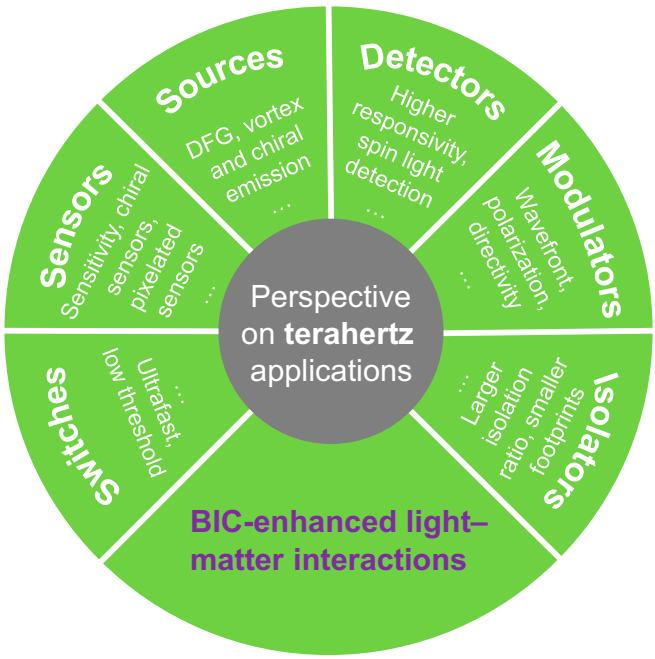

Fig. 9. Perspective of BICs on THz applications.

and specificity, and isolators with larger isolation ratio and smaller footprint [33,168,169]. Efforts to improve the performance and functionality of THz devices using novel concepts, materials, and techniques have surged in recent years [33,170]. The attractive physics of BICs and the emerging applications in shorter wavelengths would stimulate breakthroughs across all the bottlenecks in THz regime (Fig. 9). Enhanced THz generation in LN thin films based on DFG processes has been demonstrated to achieve a 17-fold improvement by BICs compared with a bare thin film [131]. The substantial enhancement of local pump energy would facilitate the miniaturization of THz sources for on-chip integration with low energy consumption. The topological features of BICs would enable the direct modulation of polarization and wavefront of THz emission, such as chiral and vortex radiation, which would benefit biosensing and multiplexing. Similar to generation of THz radiation, weak signals would be locally amplified by the strong field confinement of BICs, thereby improving the responsivities of detectors. The intrinsic polarization selectivity of BICs would exhibit a substantial discrimination ratio of spin light and provide solutions for filterless spin light detection [99,171].

The amplified local field of BICs would lead to a higher sensitivity and contribute to the development of label-free sensors in THz applications. Deep subwavelength detection of refractive index perturbation has been demonstrated in the configuration of a flexible BIC metasurface [172]. The intrinsic chirality enabled by topological charge splitting and merging of BICs could maximize the circular dichroism of THz spectrum, which would contribute to accurate characterization for pharmaceutical preparations and chiral molecules such as DNA and protein molecules [94]. More interesting studies may lead to the development of advanced sensing platforms with pixelated BIC metasurfaces and correlate the spatial information with BIC spectrum.

Inspired by the concept of nonlocal BIC metasurfaces, it would be intriguing to explore the manipulation of wavefront at specific frequency points while leaving the remaining bandwidth transparent. This approach has the potential to enable flexible shaping of THz pulses in both the spectral and spatial domains [173,174]. Polarization states as well as spin–orbit coupling of THz waves could be modulated by BICs in dielectric metasurfaces with much higher efficiency than conventional metallic counterparts [175,176]. The strategy to open a selected diffraction channel with a 0-order channel ceased by BICs will benefit THz antennas for directional emission with higher directivity.

The enhanced light–matter interactions facilitated by BICs render them highly sensitive to external perturbations, making them useful not just for sensing applications but also for ultrafast switches. Hybrid metasurfaces incorporating active media are commonly used as prototypes to demonstrate the ultrafast switches [68–70,177,178], and the ultrasensitive nature of BICs will significantly lower the threshold for an efficient modulation depth [179,180]. Ultrafast switches with low energy consumption are critical components for the next-generation THz communications [163]. Another essential component in communication systems is nonreciprocal devices, which usually rely on magneto-optical materials, leading to a large footprint of isolators or circulators. The enhanced light–matter interactions enabled by BICs could eliminate the rigid requirements of bulky magneto-optical materials or large external magnetic fields, and the smart manipulation of band dispersion of PhCs would help increase the isolation ratio [181,182]. It is expected that more efficient active devices would be developed based on BICs that could realize full control of all the properties of THz waves.

Although high-Q BICs reveal rich application prospects, the researches of BICs are still faced with some challenges. So far, most BICs in PhCs and metamaterials are theoretically localized in out-of-plane direction, while the structures are considered as an infinite lattice with periodic boundary conditions in the in-plane direction. However, perfect BICs localized in all the 3 dimensions are impossible in reality due to the finite extent of periodic lattices, which would result in a decrease of Q factors. Therefore, the actual samples often require a relatively large footprint to guarantee a high Q, which is not conducive to the miniaturization and integration of photonic devices. Recently, a mini-BIC in PhC slabs was proposed [37], which realized strong confinement in all the 3 dimensions by combining a BIC and lateral mirror for vertical localization and in-plane restriction, respectively. A record-high Q and rather small mode volume were reported in this configuration, which would significantly benefit THz applications with an enhanced Purcell factor.

At present, most experimental studies are based on quasi-BICs because they are detectable in the far field. It is quite challenging to observe true BICs as they decouple to free space. Recently, Dong et al. [183] proposed a technique to reveal the "true" photonic BICs in metasurfaces with nanometer spatial precision. The experiment utilized cathodoluminescence (CL) and monochromated electron energy loss spectroscopy (EELS) in a scanning transmission electron microscope, and excited optical modes in the near field with nanosized focused electron beams. The energy transferred in these radiative and nonradiative excitations was measured by EELS, while only radiation losses could be measured with CL in the far field. The true BIC and quasi-BIC could thus be distinguished by comparing the EELS with the CL spectra. In THz regime, near-field detection technique is rapidly developing, and novel characterization

approaches to observe true BICs and apply them are of essential importance.

In terms of radiative losses, BICs are extremely sensitive to structural defects and disorders, and a collapse of the divergent quality factors occurs if fabrication is imperfect. An extreme requirement of high-precision fabrication is necessary to access high-*Q* resonances. Developing interesting theories in addition to merging BICs and hybrid BICs would release the rigid requirement of fabrication, and THz regime is an excellent band to perform demonstration with mature fabrication and characterization techniques. In terms of nonradiative losses, they are inevitable and will lead to a severe decrease of measured *Q* factors. Looking for dielectric materials with high refractive index and low loss is an important mission to further improve the measured *Q* factors in THz regime.

In summary, the recent advances of BICs in theory and applications have demonstrated the important implications for engineering resonances in photonic devices. With the burgeoning deployment of photonics in industry, it is expected that BIC-enabled photonics will remain a very active research area and more critical progress would be achieved not only in classical optical regime but also in quantum photonics.

Acknowledgments

Funding: This work was supported by the National Natural Science Foundation of China (Award No.: 62175099), the Guangdong Basic and Applied Basic Research Foundation (Award No.: 2023A1515011085), the Stable Support Program for Higher Education Institutions from Shenzhen Science, Technology & Innovation Commission (Award No.: 20220815151149004), and startup funding of Southern University of Science and Technology.
Author contributions: L.C. initiated the idea and supervised the project. G.X. led the writing and editing with input from H.X., Junxing F, Z.X., D.L., and P.P.S. "Engineering BICs from Topological Charges" was prepared by H.X. and Junxing F. "Applications" and "Perspective on THz Applications and Conclusion" were prepared by Z.X., D.L., Junxing F., and G.X. All authors read and commented on the manuscript. **Competing interests:** The authors declare that they have no competing interests.

Data Availability

The data is available from the corresponding author upon reasonable request.

References

1. Hsu CW, Zhen B, Stone AD, Joannopoulos JD, Soljačić M. Bound states in the continuum. *Nat Rev Mater*. 2016;1:Article 16048.
2. Hsu CW, Zhen B, Lee J, Chua SL, Johnson SG, Joannopoulos JD, Soljačić M. Observation of trapped light within the radiation continuum. *Nature*. 2013;499(7457):188–191.
3. Neumann JV, Wigner E. Über merkwü rdige diskret Eigenwerte. *Phys Z*. 1929;30:465.
4. Friedrich H, Wintgen D. Interfering resonances and bound states in the continuum. *Phys Rev A*. 1985;32(6):3231–3242.
5. Marinica DC, Borisov AG, Shabanov SV. Bound states in the continuum in photonics. *Phys Rev Lett*. 2008;100(18):Article 183902.
6. Plotnik Y, Peleg O, Dreisow F, Heinrich M, Nolte S, Szameit A, Segev M. Experimental observation of optical bound states in the continuum. *Phys Rev Lett*. 2011;107(18):Article 183901.
7. Koshelev K, Bogdanov A, Kivshar Y. Engineering with bound states in the continuum. *Opt Photonics News*. 2020;31(1):38–45.
8. Koshelev K, Bogdanov A, Kivshar Y. Meta-optics and bound states in the continuum. *Sci Bull*. 2019;64(12):836–842.
9. Azzam SI, Kildishev AV. Photonic bound states in the continuum: From basics to applications. *Adv Opt Mater*. 2021;9(1):Article 2001469.
10. Joseph S, Pandey S, Sarkar S, Joseph J. Bound states in the continuum in resonant nanostructures: an overview of engineered materials for tailored applications. *Nanophotonics*. 2021;10(17):4175–4207.
11. Koshelev KL, Sadrieva ZF, Shcherbakov AA, Kivshar YS, Bogdanov AA. Bound states of the continuum in photonic structures. *Phys Usp*. 2021.
12. Cong L, Singh R. Symmetry-protected dual bound states in the continuum in metamaterials. *Adv Opt Mater*. 2019;7(13):Article 1900383.
13. Koshelev K, Lepeshov S, Liu M, Bogdanov A, Kivshar Y. Asymmetric metasurfaces with high-*Q* resonances governed by bound states in the continuum. *Phys Rev Lett*. 2018;121(19):Article 193903.
14. Sadrieva Z, Frizyuk K, Petrov M, Kivshar Y, Bogdanov A. Multipolar origin of bound states in the continuum. *Phys Rev B*. 2019;100(11):Article 115303.
15. Zhen B, Hsu CW, Lu L, Stone AD, Soljačić M. Topological nature of optical bound states in the continuum. *Phys Rev Lett*. 2014;113(25):Article 257401.
16. Mermin ND. The topological theory of defects in ordered media. *Rev Mod Phys*. 1979;51(3):591.
17. Hwang MS, Park HG, Song Q, Kivshar Y. Advancing nanolasers. *Opt Photon News*. 2023;34(1):34–41.
18. Huang C, Zhang C, Xiao S, Wang Y, Fan Y, Liu Y, Zhang N, Qu G, Ji H, Han J, et al. Ultrafast control of vortex microlasers. *Science*. 2020;367(6481):1018–1021.
19. Kodigala A, Lepetit T, Gu Q, Bahari B, Fainman Y, Kanté B. Lasing action from photonic bound states in continuum. *Nature*. 2017;541(7636):196–199.
20. Ha ST, Fu YH, Emani NK, Pan Z, Bakker RM, Paniagua-Domínguez R, Kuznetsov AI. Directional lasing in resonant semiconductor nanoantenna arrays. *Nat Nanotechnol*. 2018;13(11):1042–1047.
21. Hwang M-S, Lee H-C, Kim K-H, Jeong K-Y, Kwon S-H, Koshelev K, Kivshar Y, Park H-G. Ultralow-threshold laser using super-bound states in the continuum. *Nat Commun*. 2021;12(1):4135.
22. Yang JH, Huang ZT, Maksimov DN, Pankin PS, Timofeev IV, Hong KB, Li H, Chen JW, Hsu CY, Liu YY, et al. Low-threshold bound state in the continuum lasers in hybrid lattice resonance metasurfaces. *Laser Photonics Rev*. 2021;15(10):Article 2100118.
23. Mekis A, Chen J, Kurland I, Fan S, Villeneuve PR, Joannopoulos J. High transmission through sharp bends in photonic crystal waveguides. *Phys Rev Lett*. 1996;77(18):3787.
24. Tittl A, Leitis A, Liu M, Yesilkoy F, Choi D-Y, Neshev DN, Kivshar YS, Altug H. Imaging-based molecular barcoding with pixelated dielectric metasurfaces. *Science*. 2018;360(6393):1105–1109.

25. Leitis A, Tittl A, Liu M, Lee BH, Gu MB, Kivshar YS, Altug H. Angle-multiplexed all-dielectric metasurfaces for broadband molecular fingerprint retrieval. *Sci Adv*. 2019;5(5):eaaw2871.
26. Yesilkoy F, Arvelo ER, Jahani Y, Liu M, Tittl A, Cevher V, Kivshar Y, Altug H. Ultrasensitive hyperspectral imaging and biodetection enabled by dielectric metasurfaces. *Nat Photonics*. 2019;13(6):390–396.
27. Yang Y, Peng C, Liang Y, Li Z, Noda S. Analytical perspective for bound states in the continuum in photonic crystal slabs. *Phys Rev Lett*. 2014;113(3):Article 037401.
28. Jin J, Yin X, Ni L, Soljačić M, Zhen B, Peng C. Topologically enabled ultrahigh-*Q* guided resonances robust to out-of-plane scattering. *Nature*. 2019;574(7779):501–504.
29. Doeleman HM, Monticone F, den Hollander W, Alù A, Koenderink AF. Experimental observation of a polarization vortex at an optical bound state in the continuum. *Nat Photonics*. 2018;12(7):397–401.
30. Liu W, Wang B, Zhang Y, Wang J, Zhao M, Guan F, Liu X, Shi L, Zi J. Circularly polarized states spawning from bound states in the continuum. *Phys Rev Lett*. 2019;123(11):Article 116104.
31. Zhang Y, Chen A, Liu W, Hsu CW, Wang B, Guan F, Liu X, Shi L, Lu L, Zi J. Observation of polarization vortices in momentum space. *Phys Rev Lett*. 2018;120(18):Article 186103.
32. Yang Y, Yamagami Y, Yu X, Pitchappa P, Webber J, Zhang B, Fujita M, Nagatsuma T, Singh R. Terahertz topological photonics for on-chip communication. *Nat Photonics*. 2020;14(7):446–451.
33. Xing H, Fan J, Lu D, Gao Z, Shum PP, Cong L. Terahertz metamaterials for free-space and on-chip applications: from active metadevices to topological photonic crystals. *Adv Devices Instrum*. 2022;2022:Article 9852503.
34. Shao ZK, Chen HZ, Wang S, Mao XR, Yang ZQ, Wang SL, Wang XX, Hu X, Ma RM. A high-performance topological bulk laser based on band-inversion-induced reflection. *Nat Nanotechnol*. 2020;15(1):67–72.
35. Kumar A, Gupta M, Pitchappa P, Wang N, Szriftgiser P, Ducournau G, Singh R. Phototunable chip-scale topological photonics: 160 Gbps waveguide and demultiplexer for THz 6G communication. *Nat Commun*. 2022;13(1):5404.
36. Kang M, Mao L, Zhang S, Xiao M, Xu H, Chan CT. Merging bound states in the continuum by harnessing higher-order topological charges. *Light Sci Appl*. 2022;11(1):228.
37. Chen Z, Yin X, Jin J, Zheng Z, Zhang Z, Wang F, He L, Zhen B, Peng C. Observation of miniaturized bound states in the continuum with ultra-high quality factors. *Sci Bull*. 2022;67(4):359–366.
38. Fan J, Li Z, Xue Z, Xing H, Lu D, Xu G, Gu J, Han J, Cong L. Hybrid bound states in the continuum in terahertz metasurfaces. *Opto-Electron Sci*. 2023;2(4):Article 230006.
39. Ye W, Gao Y, Liu J. Singular points of polarizations in the momentum space of photonic crystal slabs. *Phys Rev Lett*. 2020;124(15):Article 153904.
40. Zeng Y, Hu G, Liu K, Tang Z, Qiu C-W. Dynamics of topological polarization singularity in momentum space. *Phys Rev Lett*. 2021;127(17):Article 176101.
41. Plum E, Fedotov V, Zheludev N. Optical activity in extrinsically chiral metamaterial. *Appl Phys Lett*. 2008;93(19):Article 191911.
42. Barron LD. True and false chirality and absolute asymmetric synthesis. *J Am Chem Soc*. 1986;108(18):5539–5542.
43. Yin X, Jin J, Soljačić M, Peng C, Zhen B. Observation of topologically enabled unidirectional guided resonances. *Nature*. 2020;580(7804):467–471.
44. Yin X, Peng C. Manipulating light radiation from a topological perspective. *Photonics Res*. 2020;8(11):B25–B38.
45. Khanikaev AB, Shvets G. Two-dimensional topological photonics. *Nat Photonics*. 2017;11(12):763–773.
46. Kim M, Jacob Z, Rho J. Recent advances in 2D, 3D and higher-order topological photonics. *Light Sci Appl*. 2020;9:130.
47. Wu LH, Hu X. Scheme for achieving a topological photonic crystal by using dielectric material. *Phys Rev Lett*. 2015;114(22):Article 223901.
48. Zhang Z, Lan Z, Xie Y, Chen ML, Wei E, Xu Y. Bound topological edge state in the continuum for all-dielectric photonic crystals. *Phys Rev Appl*. 2021;16(6):Article 064036.
49. Huang L, Zhang W, Zhang X. Moiré quasibound states in the continuum. *Phys Rev Lett*. 2022;128(25):Article 253901.
50. Longhi S, Valle GD. Floquet bound states in the continuum. *Sci Rep*. 2013;3:Article 2219.
51. Li C, Kartashov YV, Konotop VV. Topological Floquet bound states in the continuum. *Opt Lett*. 2022;47(19):5160–5163.
52. Benalcazar WA, Cerjan A. Bound states in the continuum of higher-order topological insulators. *Phys Rev B*. 2020;101(16):Article 161116.
53. Cerjan A, Jürgensen M, Benalcazar WA, Mukherjee S, Rechtsman MC. Observation of a higher-order topological bound state in the continuum. *Phys Rev Lett*. 2020;125(21):Article 213901.
54. Hu Z, Bongiovanni D, Jukić D, Jajtić E, Xia S, Song D, Xu J, Morandotti R, Buljan H, Chen Z. Nonlinear control of photonic higher-order topological bound states in the continuum. *Light Sci Appl*. 2021;10:Article 164.
55. Maczewsky LJ, Heinrich M, Kremer M, Ivanov SK, Ehrhardt M, Martinez F, Kartashov YV, Konotop VV, Torner L, Bauer D, et al. Nonlinearity-induced photonic topological insulator. *Science*. 2020;370(6517):701–704.
56. Kirsch MS, Zhang Y, Kremer M, Maczewsky LJ, Ivanov SK, Kartashov YV, Torner L, Bauer D, Szameit A, Heinrich M. Nonlinear second-order photonic topological insulators. *Nat Phys*. 2021;17(9):995–1000.
57. Weidemann S, Kremer M, Helbig T, Hofmann T, Stegmaier A, Greiter M, Thomale R, Szameit A. Topological funneling of light. *Science*. 2020;368(6488):311–314.
58. Hu B, Zhang Z, Zhang H, Zheng L, Xiong W, Yue Z, Wang X, Xu J, Cheng Y, Liu X, et al. Non-Hermitian topological whispering gallery. *Nature*. 2021;597(7878):655–659.
59. Li G, Zheng Y, Dutt A, Yu D, Shan Q, Liu S, Yuan L, Fan S, Chen X. Dynamic band structure measurement in the synthetic space. *Sci Adv*. 2021;7(2):Article eabe4335.
60. Minkov M, Williamson IA, Xiao M, Fan S. Zero-index bound states in the continuum. *Phys Rev Lett*. 2018;121(26):Article 263901.
61. Dong T, Liang J, Camayd-Muñoz S, Liu Y, Tang H, Kita S, Chen P, Wu X, Chu W, Mazur E, et al. Ultra-low-loss on-chip zero-index materials. *Light Sci Appl*. 2021;10:Article 10.
62. Yu N, Genevet P, Kats MA, Aieta F, Tetienne J-P, Capasso F, Gaburro Z. Light propagation with phase discontinuities: Generalized laws of reflection and refraction. *Science*. 2011;334(6054):333–337.
63. Khorasaninejad M, Chen WT, Devlin RC, Oh J, Zhu AY, Capasso F. Metalenses at visible wavelengths: Diffraction-limited

focusing and subwavelength resolution imaging. *Science*. 2016;352(6290):1190–1194.
64. Wang S, Wu PC, Su V-C, Lai Y-C, Hung Chu C, Chen J-W, Lu S-H, Chen J, Xu B, Kuan C-H. Broadband achromatic optical metasurface devices. *Nat Commun*. 2017;8(1):187.
65. Overvig A, Alù A. Diffractive nonlocal metasurfaces. *Laser Photonics Rev*. 2022;16(8):Article 2100633.
66. Chen R, Wang S. Versatile platform of nonlocal metasurfaces for both spectral and spatial control of light waves. *Light Sci Appl*. 2022;11(1):295.
67. Malek SC, Overvig AC, Alù A, Yu N. Resonant wavefront-shaping flat optics. arXiv. 2020. https://doi.org/10.48550/arXiv.2009.07054
68. Cong L, Pitchappa P, Lee C, Singh R. Active phase transition via loss engineering in a terahertz MEMS metamaterial. *Adv Mater*. 2017;29(26):Article 1700733.
69. Cong L, Pitchappa P, Wu Y, Ke L, Lee C, Singh N, Yang H, Singh R. Active multifunctional microelectromechanical system metadevices: Applications in polarization control, wavefront deflection, and holograms. *Adv Opt Mater*. 2017;5(2):Article 1600716.
70. Cong L, Srivastava YK, Zhang H, Zhang X, Han J, Singh R. All-optical active THz metasurfaces for ultrafast polarization switching and dynamic beam splitting. *Light Sci Appl*. 2018;7(1):Article 28.
71. Fan S, Suh W, Joannopoulos JD. Temporal coupled-mode theory for the Fano resonance in optical resonators. *J Opt Soc Am A*. 2003;20(3):569–572.
72. Kwon H, Sounas D, Cordaro A, Polman A, Alù A. Nonlocal metasurfaces for optical signal processing. *Phys Rev Lett*. 2018;121(17):Article 173004.
73. Song J-H, van de Groep J, Kim SJ, Brongersma ML. Non-local metasurfaces for spectrally decoupled wavefront manipulation and eye tracking. *Nat Nanotechnol*. 2021;16(11):1224–1230.
74. Koshelev K, Kruk S, Melik-Gaykazyan E, Choi J-H, Bogdanov A, Park H-G, Kivshar Y. Subwavelength dielectric resonators for nonlinear nanophotonics. *Science*. 2020;367(6475):288–292.
75. Koshelev K, Tang Y, Li K, Choi DY, Li G, Kivshar Y. Nonlinear metasurfaces governed by bound states in the continuum. *ACS Photonics*. 2019;6(7):1639–1644.
76. Overvig AC, Malek SC, Yu N. Multifunctional nonlocal metasurfaces. *Phys Rev Lett*. 2020;125(1):Article 017402.
77. Overvig AC, Malek SC, Carter MJ, Shrestha S, Yu N. Selection rules for quasibound states in the continuum. *Phys Rev B*. 2020;102(3):Article 035434.
78. Nguyen HS, Dubois F, Deschamps T, Cueff S, Pardon A, Leclercq JL, Seassal C, Letartre X, Viktorovitch P. Symmetry breaking in photonic crystals: On-demand dispersion from flatband to Dirac cones. *Phys Rev Lett*. 2018;120(6):Article 066102.
79. Malek SC, Overvig AC, Alu A, Yu N. Multifunctional resonant wavefront-shaping meta-optics based on multilayer and multi-perturbation nonlocal metasurfaces. *Light Sci Appl*. 2022;11(1):246.
80. Lan S, Zhang X, Taghinejad M, Rodrigues S, Lee K-T, Liu Z, Cai W. Metasurfaces for near-eye augmented reality. *ACS Photonics*. 2019;6(4):864–870.
81. Overvig AC, Mann SA, Alù A. Thermal metasurfaces: complete emission control by combining local and nonlocal light-matter interactions. *Phys Rev X*. 2021;11(2):Article 021050.
82. Overvig A, Alù A. Wavefront-selective Fano resonant metasurfaces. *Adv Photonics*. 2021;3(2):Article 026002.
83. Qiu CW, Zhang T, Hu G, Kivshar Y. Quo vadis, metasurfaces? *Nano Lett*. 2021;21(13):5461–5474.
84. Krasnok A, Tymchenko M, Alù A. Nonlinear metasurfaces: a paradigm shift in nonlinear optics. *Mater Today*. 2018;21(1):8–21.
85. Li G, Zhang S, Zentgraf T. Nonlinear photonic metasurfaces. *Nat Rev Mater*. 2017;2(5):Article 17010.
86. Overvig A, Yu N, Alù A. Chiral quasi-bound states in the continuum. *Phys Rev Lett*. 2021;126(7):Article 073001.
87. Chen Y, Gao J, Yang X. Chiral metamaterials of plasmonic slanted nanoapertures with symmetry breaking. *Nano Lett*. 2018;18(1):520–527.
88. Valev VK, Baumberg JJ, Sibilia C, Verbiest T. Chirality and chiroptical effects in plasmonic nanostructures: Fundamentals, recent progress, and outlook. *Adv Mater*. 2013;25(18):2517–2534.
89. Mun J, Kim M, Yang Y, Badloe T, Ni J, Chen Y, Qiu C-W, Rho J. Electromagnetic chirality: from fundamentals to nontraditional chiroptical phenomena. *Light Sci Appl*. 2020;9(1):139.
90. Gansel JK, Thiel M, Rill MS, Decker M, Bade K, Saile V, von Freymann G, Linden S, Wegener M. Gold helix photonic metamaterial as broadband circular polarizer. *Science*. 2009;325(5947):1513–1515.
91. Mark AG, Gibbs JG, Lee T-C, Fischer P. Hybrid nanocolloids with programmed three-dimensional shape and material composition. *Nat Mater*. 2013;12(9):802–807.
92. Fan J, Xiao D, Lei T, Yuan X. Incidence angle-dependent broadband chiral metamaterial for near-infrared light absorption. *J Opt Soc Am B*. 2020;37(11):3422–3428.
93. Khanikaev AB, Arju N, Fan Z, Purtseladze D, Lu F, Lee J, Sarriugarte P, Schnell M, Hillenbrand R, Belkin M. Experimental demonstration of the microscopic origin of circular dichroism in two-dimensional metamaterials. *Nat Commun*. 2016;7:Article 12045.
94. Cong L, Pitchappa P, Wang N, Singh R. Electrically programmable terahertz diatomic metamolecules for chiral optical control. *Research*. 2019;2019:Article 7084251.
95. Zhou J, Dong J, Wang B, Koschny T, Kafesaki M, Soukoulis CM. Negative refractive index due to chirality. *Phys Rev B*. 2009;79(12):Article 121104.
96. Decker M, Ruther M, Kriegler C, Zhou J, Soukoulis C, Linden S, Wegener M. Strong optical activity from twisted-cross photonic metamaterials. *Opt Lett*. 2009;34(16):2501–2503.
97. Wang Z, Jia H, Yao K, Cai W, Chen H, Liu Y. Circular dichroism metamirrors with near-perfect extinction. *ACS Photonics*. 2016;3(11):2096–2101.
98. Zhang X, Liu Y, Han J, Kivshar Y, Song Q. Chiral emission from resonant metasurfaces. *Science*. 2022;377(6611):1215–1218.
99. Wei J, Chen Y, Li Y, Li W, Xie J, Lee C, Novoselov KS, Qiu C-W. Geometric filterless photodetectors for mid-infrared spin light. *Nat Photonics*. 2023;17:171–178.
100. Cao T, Mao L, Qiu Y, Lu L, Banas A, Banas K, Simpson RE, Chui HC. Fano resonance in asymmetric plasmonic nanostructure: separation of sub-10 nm enantiomers. *Adv Opt Mater*. 2019;7(3):Article 1801172.
101. Gorkunov MV, Antonov AA, Kivshar YS. Metasurfaces with maximum chirality empowered by bound states in the continuum. *Phys Rev Lett*. 2020;125(9):Article 093903.

102. Gorkunov MV, Antonov AA, Tuz VR, Kupriianov AS, Kivshar YS. Bound states in the continuum underpin near-lossless maximum chirality in dielectric metasurfaces. *Adv Opt Mater*. 2021;9(19):Article 2100797.
103. Chen Y, Deng H, Sha X, Chen W, Wang R, Chen Y, Wu D, Chu J, Kivshar YS, Xiao S, et al. Observation of intrinsic chiral bound states in the continuum. *Nature*. 2023;613(7944):474–478.
104. Kühner L, Wendisch FJ, Antonov AA, Bürger J, Hüttenhofer L, Menezes LdS, Maier SA, Gorkunov MV, Kivshar Y, Tittl A. Unlocking the out-of-plane dimension for photonic bound states in the continuum to achieve maximum optical chirality. arXiv. 2022. https://doi.org/10.48550/arXiv.2210.05339
105. Shi T, Deng ZL, Geng G, Zeng X, Zeng Y, Hu G, Overvig A, Li J, Qiu CW, Alu A, et al. Planar chiral metasurfaces with maximal and tunable chiroptical response driven by bound states in the continuum. *Nat Commun*. 2022;13(1):Article 4111.
106. Shen Z, Fang X, Li S, Yin W, Zhang L, Chen X. Terahertz spin-selective perfect absorption enabled by quasi-bound states in the continuum. *Opt Lett*. 2022;47(3):505–508.
107. Wang J, Shi L, Zi J. Spin hall effect of light via momentum-space topological vortices around bound states in the continuum. *Phys Rev Lett*. 2022;129(23):Article 236101.
108. Iwahashi S, Kurosaka Y, Sakai K, Kitamura K, Takayama N, Noda S. Higher-order vector beams produced by photonic-crystal lasers. *Opt Express*. 2011;19(13):11963–11968.
109. Wang B, Liu W, Zhao M, Wang J, Zhang Y, Chen A, Guan F, Liu X, Shi L, Zi J. Generating optical vortex beams by momentum-space polarization vortices centred at bound states in the continuum. *Nat Photonics*. 2020;14(10):623–628.
110. Liu H, Guo C, Vampa G, Zhang JL, Sarmiento T, Xiao M, Bucksbaum PH, Vučković J, Fan S, Reis DA. Enhanced high-harmonic generation from an all-dielectric metasurface. *Nat Phys*. 2018;14(10):1006–1010.
111. McDonnell C, Deng J, Sideris S, Ellenbogen T, Li G. Functional THz emitters based on Pancharatnam-Berry phase nonlinear metasurfaces. *Nat Commun*. 2021;12(1):30.
112. Carletti L, Koshelev K, De Angelis C, Kivshar Y. Giant nonlinear response at the nanoscale driven by bound states in the continuum. *Phys Rev Lett*. 2018;121(3):Article 033903.
113. Volkovskaya I, Xu L, Huang L, Smirnov AI, Miroshnichenko AE, Smirnova D. Multipolar second-harmonic generation from high-*Q* quasi-BIC states in subwavelength resonators. *Nanophotonics*. 2020;9(12):3953–3963.
114. Ning T, Li X, Zhang Z, Huo Y, Yue Q, Zhao L, Gao Y. Ultimate conversion efficiency of second harmonic generation in all-dielectric resonators of quasi-BICs in consideration of nonlinear refraction of dielectrics. *Opt Express*. 2021;29(11):17286–17294.
115. Han Z, Ding F, Cai Y, Levy U. Significantly enhanced second-harmonic generations with all-dielectric antenna array working in the quasi-bound states in the continuum and excited by linearly polarized plane waves. *Nanophotonics*. 2021;10(3):1189–1196.
116. Anthur AP, Zhang H, Paniagua-Dominguez R, Kalashnikov DA, Ha ST, Mass TWW, Kuznetsov AI, Krivitsky L. Continuous wave second harmonic generation enabled by quasi-bound-states in the continuum on gallium phosphide metasurfaces. *Nano Lett*. 2020;20(12):8745–8751.
117. Khmelevskaia D, Markina DI, Fedorov VV, Ermolaev GA, Arsenin AV, Volkov VS, Goltaev AS, Zadiranov YM, Tzibizov IA, Pushkarev AP, et al. Directly grown crystalline gallium phosphide on sapphire for nonlinear all-dielectric nanophotonics. *Appl Phys Lett*. 2021;118(20):Article 201101.
118. Löchner FJF, Fedotova AN, Liu S, Keeler GA, Peake GM, Saravi S, Shcherbakov MR, Burger S, Fedyanin AA, Brener I, et al. Polarization-dependent second harmonic diffraction from resonant GaAs metasurfaces. *ACS Photonics*. 2018;5(5):1786–1793.
119. Vabishchevich PP, Liu S, Sinclair MB, Keeler GA, Peake GM, Brener I. Enhanced second-harmonic generation using broken symmetry III–V semiconductor fano metasurfaces. *ACS Photonics*. 2018;5(5):1685–1690.
120. Zhu D, Shao L, Yu M, Cheng R, Desiatov B, Xin CJ, Hu Y, Holzgrafe J, Ghosh S, Shams-Ansari A, et al. Integrated photonics on thin-film lithium niobate. *Adv Opt Photon*. 2021;13(2):242–352.
121. Zheng Z, Xu L, Huang L, Smirnova D, Hong P, Ying C, Rahmani M. Boosting second-harmonic generation in the $LiNbO_3$ metasurface using high-*Q* guided resonances and bound states in the continuum. *Phys Rev B*. 2022;106(12):Article 125411.
122. Zhang X, He L, Gan X, Huang X, Du Y, Zhai Z, Li Z, Zheng Y, Chen X, Cai Y, et al. Quasi-bound states in the continuum enhanced second-harmonic generation in thin-film lithium niobate. *Laser Photonics Rev*. 2022;16(9):Article 2200031.
123. Kühner L, Sortino L, Tilmann B, Weber T, Watanabe K, Taniguchi T, Maier SA, Tittl A. High-*Q* nanophotonics over the full visible spectrum enabled by hexagonal boron nitride metasurfaces. *Adv Mater*. 2023;35(13):Article 2209688.
124. Fang C, Yang Q, Yuan Q, Gu L, Gan X, Shao Y, Liu Y, Han G, Hao Y. Efficient second-harmonic generation from silicon slotted nanocubes with bound states in the continuum. *Laser Photonics Rev*. 2022;16(5):Article 2100498.
125. Zograf G, Koshelev K, Zalogina A, Korolev V, Hollinger R, Choi D-Y, Zuerch M, Spielmann C, Luther-Davies B, Kartashov D, et al. High-harmonic generation from resonant dielectric metasurfaces empowered by bound states in the continuum. *ACS Photonics*. 2022;9(2):567–574.
126. Carletti L, Kruk SS, Bogdanov AA, De Angelis C, Kivshar Y. High-harmonic generation at the nanoscale boosted by bound states in the continuum. *Phys Rev Res*. 2019;1(2):Article 023016.
127. Liu Z, Xu Y, Lin Y, Xiang J, Feng T, Cao Q, Li J, Lan S, Liu J. High-*Q* quasibound states in the continuum for nonlinear metasurfaces. *Phys Rev Lett*. 2019;123(25):Article 253901.
128. Sinev IS, Koshelev K, Liu Z, Rudenko A, Ladutenko K, Shcherbakov A, Sadrieva Z, Baranov M, Itina T, Liu J, et al. Observation of ultrafast self-action effects in quasi-BIC resonant metasurfaces. *Nano Lett*. 2021;21(20):8848–8855.
129. Yang G, Dev SU, Allen MS, Allen JW, Harutyunyan H. Optical bound states in the continuum enabled by magnetic resonances coupled to a mirror. *Nano Lett*. 2022;22(5):2001–2008.
130. Camacho-Morales R, Xu L, Zhang H, Ha ST, Krivitsky L, Kuznetsov AI, Rahmani M, Neshev D. Sum-frequency generation in high-*Q* GaP metasurfaces driven by leaky-wave guided modes. *Nano Lett*. 2022;22(15):6141–6148.
131. Hu L, Wang B, Guo Y, Du S, Chen J, Li J, Gu C, Wang L. Quasi-BIC enhanced broadband terahertz generation in all-dielectric metasurface. *Adv Opt Mater*. 2022;10(12):Article 2200193.

132. Tu Y, Sun X, Wu H, Zan X, Yang Y, Liu N, Wang X, Meng C, Lyu Z, Zhu Z, et al. Enhanced terahertz generation from the lithium niobate metasurface. *Front Phys*. 2022;10:Article 883703.
133. Luo L, Chatzakis I, Wang J, Niesler FB, Wegener M, Koschny T, Soukoulis CM. Broadband terahertz generation from metamaterials. *Nat Commun*. 2014;5:Article 3055.
134. McDonnell C, Deng J, Sideris S, Li G, Ellenbogen T. Terahertz metagrating emitters with beam steering and full linear polarization control. *Nano Lett*. 2022;22(7):2603–2610.
135. Lu Y, Feng X, Wang Q, Zhang X, Fang M, Sha WEI, Huang Z, Xu Q, Niu L, Chen X, et al. Integrated terahertz generator-manipulators using epsilon-near-zero-hybrid nonlinear metasurfaces. *Nano Lett*. 2021;21(18):7699–7707.
136. Liu Z, Wang J, Chen B, Wei Y, Liu W, Liu J. Giant enhancement of continuous wave second harmonic generation from few-layer GaSe coupled to High-*Q* quasi bound states in the continuum. *Nano Lett*. 2021;21(17):7405–7410.
137. Wang T, Zhang S. Large enhancement of second harmonic generation from transition-metal dichalcogenide monolayer on grating near bound states in the continuum. *Opt Express*. 2018;26(1):322–337.
138. Liu Y, Zhu S, Zhou Q, Cao Y, Fu Y, Gao L, Chen H, Xu Y. Enhanced third-harmonic generation induced by nonlinear field resonances in plasmonic-graphene metasurfaces. *Opt Express*. 2020;28(9):13234–13242.
139. Bernhardt N, Koshelev K, White SJU, Meng KWC, Froch JE, Kim S, Tran TT, Choi DY, Kivshar Y, Solntsev AS. Quasi-BIC resonant enhancement of second-harmonic generation in WS_2 monolayers. *Nano Lett*. 2020;20(7):5309–5314.
140. Löchner FJF, George A, Koshelev K, Bucher T, Najafidehaghani E, Fedotova A, Choi D-Y, Pertsch T, Staude I, Kivshar Y, et al. Hybrid dielectric metasurfaces for enhancing second-harmonic generation in chemical vapor deposition grown MoS_2 monolayers. *ACS Photonics*. 2021;8(1):218–227.
141. Hong P, Xu L, Rahmani M. Dual bound states in the continuum enhanced second harmonic generation with transition metal dichalcogenides monolayer. *Opto-Electron Adv*. 2022;5(7):Article 200097.
142. Wang J, Clementi M, Minkov M, Barone A, Carlin J-F, Grandjean N, Gerace D, Fan S, Galli M, Houdré R. Doubly resonant second-harmonic generation of a vortex beam from a bound state in the continuum. *Optica*. 2020;7(9):1126–1132.
143. Mobini E, Alaee R, Boyd RW, Dolgaleva K. Giant asymmetric second-harmonic generation in bianisotropic metasurfaces based on bound states in the continuum. *ACS Photonics*. 2021;8(11):3234–3240.
144. Xiao S, Qin M, Duan J, Wu F, Liu T. Polarization-controlled dynamically switchable high-harmonic generation from all-dielectric metasurfaces governed by dual bound states in the continuum. *Phys Rev B*. 2022;105(19):Article 195440.
145. Xu L, Zangeneh Kamali K, Huang L, Rahmani M, Smirnov A, Camacho-Morales R, Ma Y, Zhang G, Woolley M, Neshev D, et al. Dynamic nonlinear image tuning through magnetic dipole quasi-BIC ultrathin resonators. *Adv Sci*. 2019;6(15):Article 1802119.
146. Liu Q, Cheng B, Chao M, Zhang W, Xu Y, Song G. Giant nonlinear circular dichroism from high *Q*-factor asymmetric lithium niobate metasurfaces. *Ann Phys*. 2021;533(11):Article 2100255.
147. Kruk SS, Wang L, Sain B, Dong Z, Yang J, Zentgraf T, Kivshar Y. Asymmetric parametric generation of images with nonlinear dielectric metasurfaces. *Nat Photonics*. 2022;16(8):561–565.
148. Baranov DG, Zuev DA, Lepeshov SI, Kotov OV, Krasnok AE, Evlyukhin AB, Chichkov BN. All-dielectric nanophotonics: The quest for better materials and fabrication techniques. *Optica*. 2017;4(7):814–825.
149. Yang Q, Liu Y, Gan X, Fang C, Han G, Hao Y. Nonlinear bound states in the continuum of etchless lithium niobate metasurfaces. *IEEE Photonics J*. 2020;12(5):1–9.
150. Huang Z, Luo K, Feng Z, Zhang Z, Li Y, Qiu W, Guan H, Xu Y, Li X, Lu H. Resonant enhancement of second harmonic generation in etchless thin film lithium niobate heteronanostructure. *Sci China Phys Mech Astron*. 2022;65(10):Article 104211.
151. Aigner A, Tittl A, Wang J, Weber T, Kivshar Y, Maier SA, Ren H. Plasmonic bound states in the continuum to tailor light-matter coupling. *Sci Adv*. 2022;8(49):Article eadd4816.
152. Cong L, Tan S, Yahiaoui R, Yan F, Zhang W, Singh R. Experimental demonstration of ultrasensitive sensing with terahertz metamaterial absorbers: A comparison with the metasurfaces. *Appl Phys Lett*. 2015;106(3):Article 031107.
153. Cong L, Manjappa M, Xu N, Al-Naib I, Zhang W, Singh R. Fano resonances in terahertz metasurfaces: a figure of merit optimization. *Adv Opt Mater*. 2015;3(11):1537–1543.
154. Romano S, Zito G, Torino S, Calafiore G, Penzo E, Coppola G, Cabrini S, Rendina I, Mocella V. Label-free sensing of ultralow-weight molecules with all-dielectric metasurfaces supporting bound states in the continuum. *Photonics Res*. 2018;6(7):726–733.
155. Singh R, Cao W, Al-Naib I, Cong L, Withayachumnankul W, Zhang W. Ultrasensitive terahertz sensing with high-*Q* Fano resonances in metasurfaces. *Appl Phys Lett*. 2014;105(17):Article 171101.
156. Romano S, Zito G, Managò S, Calafiore G, Penzo E, Cabrini S, De Luca AC, Mocella V. Surface-enhanced raman and fluorescence spectroscopy with an all-dielectric metasurface. *J Phys Chem C*. 2018;122(34):19738–19745.
157. Hill MT, Gather MC. Advances in small lasers. *Nat Photonics*. 2014;8(12):908–918.
158. Ma R-M, Oulton RF. Applications of nanolasers. *Nat Nanotechnol*. 2019;14(1):12–22.
159. Bahari B, Vallini F, Lepetit T, Tellez-Limon R, Park J, Kodigala A, Fainman Y, Kante B. Integrated and steerable vortex lasers using bound states in continuum. arXiv. 2017. https://doi.org/10.48550/arXiv.1707.00181
160. Wu M, Ha ST, Shendre S, Durmusoglu EG, Koh W-K, Abujetas DR, Sánchez-Gil JA, Paniagua-Domínguez R, Demir HV, Kuznetsov AI. Room-temperature lasing in colloidal nanoplatelets via mie-resonant bound states in the continuum. *Nano Lett*. 2020;20(8):6005–6011.
161. Zhen B, Chua S-L, Lee J, Rodriguez AW, Liang X, Johnson SG, Joannopoulos JD, Soljačić M, Shapira O. Enabling enhanced emission and low-threshold lasing of organic molecules using special Fano resonances of macroscopic photonic crystals. *Proc Natl Acad Sci*. 2013;110(34):13711–13716.
162. Sun T, Kan S, Marriott G, Chang-Hasnain C. High-contrast grating resonators for label-free detection of disease biomarkers. *Sci Rep*. 2016;6(1):Article 27482.
163. Sarieddeen H, Saeed N, Al-Naffouri TY, Alouini MS. Next generation terahertz communications: a rendezvous of

sensing, imaging, and localization. *IEEE Commun Mag*. 2020;58(5):69–75.
164. Zhang D, Kroh T, Ritzkowsky F, Rohwer T, Fakhari M, Cankaya H, Calendron A-L, Matlis NH, Kärtner FX. THz-enhanced DC ultrafast electron diffractometer. *Ultrafast Sci*. 2021;2021:Article 9848526.
165. Tonouchi M. Cutting-edge terahertz technology. *Nat Photonics*. 2007;1(2):97–105.
166. Nagatsuma T, Ducournau G, Renaud CC. Advances in terahertz communications accelerated by photonics. *Nat Photonics*. 2016;10(6):371–379.
167. Taday PF. Applications of terahertz spectroscopy to pharmaceutical sciences. *Philos Trans R Soc London, Ser A*. 2004;362(1815):351–363.
168. Lewis RA. A review of terahertz sources. *J Phys D Appl Phys*. 2014;47(37):Article 374001.
169. Salamin Y, Benea-Chelmus I-C, Fedoryshyn Y, Heni W, Elder DL, Dalton LR, Faist J, Leuthold J. Compact and ultra-efficient broadband plasmonic terahertz field detector. *Nat Commun*. 2019;10(1):Article 5550.
170. E Y, Zhang L, Tcypkin A, Kozlov S, Zhang C, Zhang X-C. Broadband THz sources from gases to liquids. *Ultrafast Sci*. 2021;2021:Article 9891762.
171. Kühner L, Sortino L, Berté R, Wang J, Ren H, Maier SA, Kivshar Y, Tittl A. Radial bound states in the continuum for polarization-invariant nanophotonics. *Nat Commun*. 2022;13(1):Article 4992.
172. Srivastava YK, Ako RT, Gupta M, Bhaskaran M, Sriram S, Singh R. Terahertz sensing of 7 nm dielectric film with bound states in the continuum metasurfaces. *Appl Phys Lett*. 2019;115(15):Article 151105.
173. Cong L, Han J, Zhang W, Singh R. Temporal loss boundary engineered photonic cavity. *Nat Commun*. 2021;12(1): Article 6940.
174. Cong L, Singh R. Spatiotemporal dielectric metasurfaces for unidirectional propagation and reconfigurable steering of terahertz beams. *Adv Mater*. 2020;32(28):Article 2001418.
175. Cong L, Cao W, Zhang X, Tian Z, Gu J, Singh R, Han J, Zhang W. A perfect metamaterial polarization rotator. *Appl Phys Lett*. 2013;103(17):Article 171107.
176. Cong L, Xu N, Gu J, Singh R, Han J, Zhang W. Highly flexible broadband terahertz metamaterial quarter-wave plate. *Laser Photonics Rev*. 2014;84):626–632.
177. Cong L, Xu N, Han J, Zhang W, Singh R. A tunable dispersion-free terahertz metadevice with pancharatnam–berry-phase-enabled modulation and polarization control. *Adv Mater*. 2015;27(42):6630–6636.
178. Cong L, Srivastava YK, Solanki A, Sum TC, Singh R. Perovskite as a platform for active flexible metaphotonic devices. *ACS Photonics*. 2017;4(7):1595–1601.
179. Han S, Cong L, Srivastava YK, Qiang B, Rybin MV, Kumar A, Jain R, Lim WX, Achanta VG, Prabhu SS, et al. All-dielectric active terahertz photonics driven by bound states in the continuum. *Adv Mater*. 2019;31(37):Article 1901921.
180. Fan K, Shadrivov IV, Padilla WJ. Dynamic bound states in the continuum. *Optica*. 2019;6(2):169–173.
181. Bi L, Hu J, Jiang P, Kim DH, Dionne GF, Kimerling LC, Ross CA. On-chip optical isolation in monolithically integrated non-reciprocal optical resonators. *Nat Photonics*. 2011;5(12):758–762.
182. Ignatyeva DO, Belotelov VI. Bound states in the continuum enable modulation of light intensity in the Faraday configuration. *Opt Lett*. 2020;45(23):6422–6425.
183. Dong Z, Mahfoud Z, Paniagua-Domínguez R, Wang H, Fernández-Domínguez AI, Gorelik S, Ha ST, Tjiptoharsono F, Kuznetsov AI, Bosman M, et al. Nanoscale mapping of optically inaccessible bound-states-in-the-continuum. *Light Sci Appl*. 2022;11(1):Article 20.